

CHALMERS
UNIVERSITY OF TECHNOLOGY

Methanol mediated CO_2 hydrogenation to lower olefins

Experiments and kinetic modelling

Master's thesis in Innovative and Sustainable Chemical Engineering

Arvid Lundström

DEPARTMENT OF CHEMISTRY AND CHEMICAL ENGINEERING

CHALMERS UNIVERSITY OF TECHNOLOGY
Gothenburg, Sweden 2021
www.chalmers.se

Master's thesis 2021

Methanol mediated CO_2 hydrogenation to lower olefins

Experiments and kinetic modelling

Arvid Lundström



CHALMERS
UNIVERSITY OF TECHNOLOGY

Department of Chemistry and Chemical Engineering
Division of Chemical Engineering
Competence Center for Catalysis (KCK)
Chalmers University of Technology
Gothenburg, Sweden 2021

Methanol mediated CO_2 hydrogenation to lower olefins
Experiments and kinetic modelling
Arvid Lundström

© Arvid Lundström, 2021.

Supervisor: Sreetama Ghosh, Department of Chemistry and Chemical Engineering
Supervisor: Wei Di, Department of Chemistry and Chemical Engineering
Examiner: Derek Creaser, Department of Chemistry and Chemical Engineering

Master's Thesis 2021
Department of Chemistry and Chemical Engineering
Division of Chemical Engineering
Competence Center for Catalysis (KCK)
Chalmers University of Technology
SE-412 96 Gothenburg
Telephone +46 31 772 1000

Typeset in LaTeX
Gothenburg, Sweden 2021

Methanol mediated CO_2 hydrogenation to lower olefins
Experiments and kinetic modelling
Arvid Lundström
Department of Chemistry and Chemical Engineering
Chalmers University of Technology

Abstract

Hydrogenation of CO_2 into useful chemicals like lower olefins is of great interest as a solution for utilising the CO_2 from carbon capture technologies. In this work a LHHW kinetic model of methanol mediated catalytic hydrogenation of CO_2 to lower olefins has been developed, which is the first of its kind. To develop the model experiments on a reactor were preformed over different temperatures, pressures, weight hourly space velocity and H_2:CO_2 molar feed ratio of the system. The input reactants were only H_2 and CO_2 and no other species. Parameter optimisation was performed in order to determine the kinetic parameters values based on minimising the residual sum of squares. The model predicts the data well and that the methanol synthesis is rate limiting for the formation of olefins when the reactor is operated at high temperatures. The yield of lower olefins was the highest when the reactor was 325-350°C, 30 bar pressure, low WHSV and high H_2:CO_2 ratio. At very high temperatures and pressures the hydrogenation of olefins reduced the olefin yield and the CO_2 conversion was worsened by low temperature and low pressure. Analysis of the experiments showed signs of deactivation of the catalyst during experiments, which resulted in significant variance for repeated experiments, reducing the reliability of the model without further validation by experiments. Nevertheless, the developed experimental model could predict the available data well and can be a starting point for more research into this topic.

Keywords: Carbon capture and utilisation (CCU), LHHW kinetics, CO_2 hydrogenation, kinetic modeling, SSZ-13, In_2O_3.

Acknowledgements

Without the assistance of several people the completion of this thesis would not be achieved. I would like to thank my main supervisor Sreetama Ghosh that has helped with many aspects of the project. I have her to thank for making sure i had a steady ground to stand on before i started working and especially was she important in the experimental work. I would also like to thank my other supervisor Wei Di who has helped me understand how the catalyst works. He was also the one that synthesised the catalyst and provided me the X-ray diffraction results.

Thanks to the Swedish Energy Agency, Perstorp Group and the Västsvenska kemi- och materialklustret for their support of this research, in particular Oleg Pajalic from Perstorp and Lars Josefsson from the Västsvenska kemi- och materialklustret. My gratitude goes to Derek Creaser for giving me this opportunity to work with this exciting topic and with the helpful insights in modelling, LHHW kinetics and analysing the results. Thanks to Louise Olsson for helping with lab safety. Lastly, I would like to thank everybody else who has helped and contributed to the completion of this thesis.

Arvid Lundström, Gothenburg, May 2021

Contents

List of Figures **xi**

List of Tables **xv**

1 Introduction **1**

2 Theory **3**
2.1 Langmuir-Hinshelwood-Hougen-Watson kinetics . . . 3
2.2 Carbon dioxide hydrogenation to methanol . . . 5
2.2.1 Mechanism . . . 5
2.2.2 Kinetic model . . . 5
2.3 Methanol to lower olefins . . . 6
2.3.1 SSZ-13 and other zeolites . . . 6
2.3.2 Kinetic model . . . 7
2.3.3 Mechanism . . . 8
2.4 In_2O_3/SSZ-13 bifunctional catalyst . . . 8

3 Methods **11**
3.1 Experimental work . . . 11
3.1.1 Catalyst synthesis . . . 11
3.1.2 Catalyst characterisation . . . 12
3.1.3 Catalytic activity tests . . . 12
3.1.4 Analysis of experiments . . . 13
3.1.4.1 Gas chromatography . . . 13
3.1.4.2 Calculations for analysing experimental results . . . 13
3.2 Mathematical modelling . . . 14
3.2.1 Reactor model . . . 14
3.2.2 Reaction kinetics . . . 15
3.2.3 Parameter optimisation . . . 17
3.2.4 Analysis of the model . . . 18

4 Results and discussion **21**
4.1 Experimental results . . . 21
4.1.1 Catalyst characterisation . . . 21
4.1.2 Catalytic activity . . . 22
4.1.2.1 The influence of temperature on catalytic activity . . . 25

4.1.2.2 The influence of residence time on catalytic activity . 27
4.1.2.3 The influence of H_2:CO_2 ratio on catalytic activity . 28
4.1.2.4 Stability of catalyst 29
4.2 Mathematical modelling 30
4.2.1 Determination of kinetic parameter values 30
4.2.2 Comparison of model predictions with experiments 32
4.2.2.1 Olefins predictions compared with experimental results 33
4.2.2.2 Paraffin predictions compared with experimental results 34
4.2.2.3 Methanol and methane predictions compared with experimental results 35
4.2.2.4 CO predictions compared with experimental results . 37
4.2.2.5 CO_2 predictions compared with experimental results 39
4.2.3 Model residual plots 40
4.2.4 Possibilities for improving the model 41
4.3 Further work in this topic 42

5 Conclusion **45**

Bibliography **47**

A Appendix - Reactor model assumptions **I**
A.1 Estimation of physical properties I
A.1.1 Fluid density I
A.1.2 Fluid viscosity I
A.1.3 Diffusivity II
A.2 Pressure drop calculation II
A.3 Mears parameter calculation II
A.4 Weisz-Prater parameter calculation III

B Appendix - Results **V**
B.1 Experimental results V
B.1.0.1 The influence of total pressure on catalytic activity . V
B.2 Model residual plots VII
B.2.1 Olefin residual plots VII
B.2.2 Paraffin residual plots IX
B.2.3 Methanol residual plots XII
B.2.4 Methane residual plots XIV
B.2.5 CO residual plots XVI
B.2.6 CO_2 residual plots XVIII

C Appendix - Mass transfer model **XXI**
C.1 Model description XXI
C.1.1 Reactor model XXI
C.1.2 Catalyst particle model XXII
C.1.3 Model Implementation XXII
C.2 Results XXIII

List of Figures

4.1 XRD patterns for In_2O_3 **(a)** and SSZ-13 zeolite **(b)**. 21

4.2 Carbon selectivities and CO_2 conversion calculated with equation 3.3 and equation 3.2 respectively over different reactor temperatures. Experiments included are 1a to 1g and 5a to 5d. 25

4.3 Molar based hydrocarbon distribution over different temperatures. Note that CH_4 is not included among paraffins. Experiments included are 1a to 1g and 5a to 5d. 26

4.4 Carbon selectivities and CO_2 conversion calculated with equation 3.3 and equation 3.2 respectively over different weight hourly space velocity. Experiments included are 4a, 4b, 4c and 4d. 27

4.5 Molar based hydrocarbon distribution over different WHSV. Note that CH_4 is not included among paraffins. Experiments included are 4a, 4b, 4c and 4d. 28

4.6 Carbon selectivities and CO_2 conversion calculated with equation 3.3 and equation 3.2 respectively over different H_2:CO_2 ratios. Experiments included are 3a, 3b and 3c. 28

4.7 Molar based hydrocarbon distribution over different H_2:CO_2 ratios. Note that CH_4 is not included among paraffins. Experiments included are 3a, 3b and 3c. 29

4.8 CO_2 conversion and carbon selectivities at standard reactor conditions calculated with equation 3.3 and equation 3.2 respectively over the time that the reactor was operated. 30

4.9 Model predictions of various olefin molar fractions compared with the experimental results for varying temperature **(a)**, total pressure **(b)**, WHSV **(c)** and H_2:CO_2 molar feed ratio **(d)**. Unless otherwise indicated conditions are 300°C, 30 bar, 6000 Nml/g/h and 3:1 H_2:CO_2 molar feed ratio. 33

4.10 Model predictions of various paraffin molar fractions compared with the experimental results for varying temperature **(a)**, total pressure **(b)**, WHSV **(c)** and H_2:CO_2 molar feed ratio **(d)**. Unless otherwise indicated conditions are 300°C, 30 bar, 6000 Nml/g/h and 3:1 H_2:CO_2 molar feed ratio. 35

4.11 Model predictions of methanol and methane molar fractions compared with the experimental results for varying temperature **(a)**, total pressure **(b)**, WHSV **(c)** and H_2:CO_2 molar feed ratio **(d)**. Unless otherwise indicated conditions are 300°C, 30 bar, 6000 Nml/g/h and 3:1 H_2:CO_2 molar feed ratio. 36
4.12 Model predictions of CO molar fraction compared with the experimental results for varying temperature **(a)**, total pressure **(b)**, WHSV **(c)** and H_2:CO_2 molar feed ratio **(d)**. Unless otherwise indicated conditions are 300°C, 30 bar, 6000 Nml/g/h and 3:1 H_2:CO_2 molar feed ratio. 37
4.13 Model predictions of CO_2 molar fraction compared with the experimental results for varying temperature **(a)**, total pressure **(b)**, WHSV **(c)** and H_2:CO_2 molar feed ratio **(d)**. Unless otherwise indicated conditions are 300°C, 30 bar, 6000 Nml/g/h and 3:1 H_2:CO_2 molar feed ratio. The model prediction for H_2 is also shown. 39
4.14 Residuals of olefins defined in equation 3.23 plotted along reactor temperature. 40
4.15 Residuals of olefins defined in equation 3.23 over the chronological order the experiment was conducted. 41

B.1 Carbon selectivities and CO_2 conversion calculated with equation 3.3 and equation 3.2 respectively over different reactor pressures. Experiments included are 2a, 2b, 2c, 5e and 5f. V
B.2 Molar based hydrocarbon distribution over different pressures. Note that CH_4 is not included among paraffins. Experiments included are 2a, 2b, 2c, 5e and 5f. VI
B.3 Residuals of olefins defined in equation 3.23 plotted along reactor pressure. VII
B.4 Residuals of olefins defined in equation 3.23 plotted along WHSV. . . VIII
B.5 Residuals of olefins defined in equation 3.23 plotted along H_2:CO_2 ratio.VIII
B.6 Residuals of paraffins defined in equation 3.23 plotted along reactor temperature. IX
B.7 Residuals of paraffins defined in equation 3.23 over the chronological order the experiments were conducted. X
B.8 Residuals of paraffins defined in equation 3.23 plotted along reactor pressure. X
B.9 Residuals of paraffins defined in equation 3.23 plotted along WHSV. . XI
B.10 Residuals of paraffins defined in equation 3.23 plotted along H_2:CO_2 ratio. XI
B.11 Residual plots of methanol defined in equation 3.23 over different reactor conditions XII
B.12 Residuals of methanol defined in equation 3.23 over the chronological order of the experiments were conducted. XIII
B.13 Residual plots defined in equation 3.23 of methane over different reactor conditions XIV

B.14 Residuals of methane defined in equation 3.23 over the chronological order of the experiments were conducted. XV
B.15 Residual plots defined in equation 3.23 of CO over different reactor conditions XVI
B.16 Residuals of CO defined in equation 3.23 over the chronological order of the experiments were conducted. XVII
B.17 Residual plots as defined in equation 3.23 of CO_2 over different reactor conditions XVIII
B.18 Residuals of CO_2 defined in equation 3.23 over the chronological order of the experiments was conducted. XIX

C.1 Concentration over length from catalyst centre of various species. From top left: H_2, CO_2, MeOH, CO, CH_4, DME and H_2O. XXIII
C.2 Reactor simulation results. XXIV

List of Tables

2.1 Reaction constants, activation energies, adsorption constants and enthalpy of adsorption from the model developed by Ghosh *et al.* [13]. Reaction- and adsorption constants are for 300 °C. 6

3.1 Response factors used to convert the GC results to molar fractions. Calibration has been done externally. 13
3.2 Summary of all reactions used in the modelling. 16

4.1 Experimental conditions for the different experiments conducted. . . . 22
4.2 CO_2 conversion, carbon selectivity and carbon balance for all experiments calculated with equation 3.3, equation 3.2 and equation 3.4 respectively. HC stands for hydrcocarbons, Ol stands for olefins, Pf stands for paraffins and C_B is the carbon balance. 23
4.3 Molar fraction variance of different species measured as defined in equation 3.5. H_2, DME and water are not measured and therefore not included. 24
4.4 Reference rate constants for the final model and their normalised sensitivity coefficient. 31
4.5 Activation energies for the final model and their normalised sensitivity coefficient. 31
4.6 The empirical factors from equation 3.13 for the final model and their normalised sensitivity coefficient. 32
4.7 Reference adsorption equilibrium constants and heat of adsorption for the final model and their normalised sensitivity coefficient. 32

1
Introduction

As the use of fossil fuels increases worldwide, the CO_2 emission into the atmosphere has increased as well [1]. This means that the negative effect of these emissions such as global warming and ocean acidification also will increase [1]. In recent years, greenhouse gas emissions such as CO_2 has been an increasing concern globally and therefore there exists a great interest to reduce the amount of greenhouse gases in the atmosphere [2]. In 2015, world leaders pledged to restrict global warming to 1-2 °C via the Paris agreement [3]. This will likely lead to increased restrictions on emission of CO_2 such as taxes on CO_2 emissions. Therefore, technologies that can reduce CO_2 emissions significantly need to be developed. One such technology is called carbon capture and storage (CCS), which aims to collect and store CO_2 from different sources [3]. Unfortunately, CCS is currently not commercially viable and also is inhibited by geography and by the fact that it does not add intrinsic value as it treats CO_2 as waste [4]. Therefore, CCS needs strong regulation to be commercially viable [4].

Another possible path is to utilise the carbon in CO_2 to make chemicals with intrinsic value, which is called carbon capture and utilisation (CCU) [2]. As CO_2 is an ubiquitous and non-toxic chemical, it has the potential to be an environmentally friendly feedstock to many different chemicals. By using hydrogen produced from water electrolysis using renewable energy or a side product from an existing process as the second feedstock chemical, many different chemicals can be produced without using fossile based resources [1, 2]. The main challenges of CO_2 hydrogenation is that CO_2 is thermodynamically stable and kinetically inert, meaning that CCU will require large amounts of energy [2].

A vast amount of chemicals such as methanol, dimethyl ether (DME) and hydrocarbons like liquid fuels, aromatics and lower olefins have the possibility to be produced from hydrogenation of CO_2 [2]. In this project, the goal is to synthesise lower olefins from CO_2 and H_2 in industrially relevant conditions. Lower olefins ($C_2^= - C_4^=$) such as ethylene, propylene and butylene are very important intermediates in the production of plastics, synthetic fibres, rubbers, solvents and other chemicals [4, 5]. Ethylene is mainly used to produce polyethylene but also polyethylene terephalate (PET) and polyvinyl chloride (PVC) [4]. Propylene is mainly used to produce the plastics polypropylene (PP) and propylene oxide as well as the solvent Cumene [4]. At the moment, the majority of lower olefins is produced by steam cracking of alkanes which is fossil based and some from natural gas via methanol, which is also fossil based [5].

There are several possible paths to synthesise olefins by hydrogenation of CO_2. One is to synthesise methanol (CH_3OH) in one step and then to transform the methanol to olefins (MTO) in separate stages [1–6]. Another is to use the reverse water gas shift (RWGS) reaction to reduce CO_2 to CO and then utilise a Fischer-Tropsch synthesis (FTS) in a separate step to produce olefins [1–6]. Both these paths require at least two reactor steps with separation in between. Therefore, it would be favourable to achieve the same synthesis but in a single step. That can be done using either the FTS or the methanol mediated pathway. In this project, a bifunctional catalyst consisting of In_2O_3 and the zeolite SSZ-13 has been used to produce lower olefins directly via a methanol mediated pathway.

Kinetic modelling has the ability to predict the performance of a certain catalyst. This is very helpful in the design of reactors as the behaviour of the reactor will be easier to predict and less efforts will be required when scaling up the reactor. But this requires development of accurate models. The purpose of this project is to develop an accurate kinetic model for CO_2 hydrogenation to lower olefins using Langmuir-Hinshelwood-Hougen-Watson (LHHW) kinetics. At the moment, there are no studies found in literature on the kinetic modelling of methanol mediated CO_2 hydrogenation to olefins [2].

2
Theory

As the aim of this thesis is to develop a kinetic model on the hydrogenation of CO_2 to lower olefins, an understanding of the nature of the reactions involved as well as how the rate expression can be derived from a given rate determining mechanistic step is important. Therefore this literature review goes through the mathematics of Langmuir-Hinshelwood-Hougen-Watson (LHHW) kinetics, the mechanisms of the reactions as well as other factors important for realising hydrogenation of CO_2 to lower olefins.

2.1 Langmuir-Hinshelwood-Hougen-Watson kinetics

To describe the kinetics of these catalytic reactions the Langmuir–Hinshelwood–Hougen–Watson (LHHW) reaction mechanism has been considered. LHHW kinetic expression can be used when there is a chemical reaction occurring in a heterogeneous solid catalyst surface and assuming that one elementary reaction step is rate determining and that all other reactions steps are in equilibrium [7]. Let use the following general reaction as an example:

$$\mathrm{A} + \mathrm{B} \rightleftharpoons \mathrm{C} + \mathrm{D}. \tag{2.1}$$

And then let S be the concentration of unoccupied sites, S_0 be the total active sites occupied by all species and S_i be the active sites occupied by specie i. The following are all the elementary steps involved in the example reaction:

$$\mathrm{A} + \mathrm{S} \underset{k_1'}{\overset{k_1}{\rightleftharpoons}} (\mathrm{A} \cdot \mathrm{S}) \tag{2.2}$$

$$\mathrm{B} + \mathrm{S} \underset{k_2'}{\overset{k_2}{\rightleftharpoons}} (\mathrm{B} \cdot \mathrm{S}) \tag{2.3}$$

$$(\mathrm{A} \cdot \mathrm{S}) + (\mathrm{B} \cdot \mathrm{S}) \underset{k_3'}{\overset{k_3}{\rightleftharpoons}} (\mathrm{C} \cdot \mathrm{S}) + (\mathrm{D} \cdot \mathrm{S}) \tag{2.4}$$

$$(\mathrm{C} \cdot \mathrm{S}) \underset{k_4'}{\overset{k_4}{\rightleftharpoons}} \mathrm{C} + \mathrm{S} \tag{2.5}$$

$$(\mathrm{D} \cdot \mathrm{S}) \underset{k_5'}{\overset{k_5}{\rightleftharpoons}} \mathrm{D} + \mathrm{S}. \tag{2.6}$$

Where equation 2.2 and 2.3 are adsorption of reactants, equation 2.4 is the surface reaction and equation 2.5 and 2.6 are desorption of products. Assuming that the surface reaction is rate determining gives

$$r = k_3 S_A S_B - k_3^{'} S_C S_D, \tag{2.7}$$

and assuming that the other reactions are in equilibrium gives.

$$\frac{S_A}{p_A \cdot S} = K_1 = \frac{k_1}{k_1^{'}}, \tag{2.8}$$

$$\frac{S_B}{p_B \cdot S} = K_2 = \frac{k_2}{k_2^{'}}, \tag{2.9}$$

$$\frac{S_C}{p_C \cdot S} = K_4 = \frac{k_4^{'}}{k_4}, \tag{2.10}$$

$$\frac{S_D}{p_D \cdot S} = K_5 = \frac{k_5^{'}}{k_5}. \tag{2.11}$$

Where p_i is the partial pressure of species i. Then the rate expression can be rewritten as

$$r = k_3(K_1 \cdot p_A \cdot S) \cdot (K_2 \cdot p_B \cdot S) - k_3^{'}(K_4 \cdot p_C \cdot S) \cdot (K_5 \cdot p_D \cdot S) \tag{2.12}$$

$$r = k_3 K_1 K_2 \left(p_a p_B - \frac{K_4 K_5}{K_1 K_2 K_{eq}} p_C p_D \right) S^2. \tag{2.13}$$

Where $K_{eq} = \frac{k_3}{k_3^{'}}$. The number of sites occupied is

$$S_0 = S + S_A + S_B + S_C + S_D, \tag{2.14}$$

$$S_0 = S + K_1 \cdot p_A \cdot S + K_2 \cdot p_B \cdot S + K_4 \cdot p_C \cdot S + K_5 \cdot p_D \cdot S, \tag{2.15}$$

$$S = \frac{S_0}{1 + K_1 p_A + K_2 p_B + K_4 p_C + K_5 p_D}. \tag{2.16}$$

As k_3, K_1, K_2 and S_0 all are properties of the catalyst, they can be lumped into one rate constant. Let $k = k_3 K_1 K_2 S_0^2$, which gives the final rate expression.

$$r = \frac{k \left(p_A p_B - \frac{p_C p_D}{K_{eq}} \right)}{(1 + K_1 p_A + K_2 p_B + K_4 p_C + K_5 p_D)^2} \tag{2.17}$$

Equation 2.17 is specific for the example but it can used to explain LHHW kinetics more generally. This general rate expression can be split into three parts, one kinetic term, one driving force term and one inhibition term. The kinetic term is usually only the rate constant, the driving force is a term including the partial pressures (or concentrations) of the species and the thermodynamical equilibrium constant of the overall reaction and the inhibition term describes the inhibiting effect the adsorbed species may have if they occupy the active sites. The exponent to the inhibition term is dependent on how many sites are involved in the surface reaction, which is two in the example but could be any number of sites.

2.2 Carbon dioxide hydrogenation to methanol

In this thesis, a bifunctional catalyst containing In_2O_3 and SSZ-13 zeolite will be used to perform hydrogenation of CO_2 to lower olefins. This section will cover the reactions that the In_2O_3 catalyst catalyses. In_2O_3 has been proven to be a superior catalyst for CO_2 hydrogenation to methanol with high selectivity at industry relevant conditions [8]. This is mainly due to its high concentration of oxygen vacancies that has the ability to to activate CO_2 [8]. Hydrogenation over the solid catalyst is believed to involve the following reactions: [9, 10]

$$CO_2 + 3H_2 \rightleftharpoons CH_3OH + H_2O \tag{2.18}$$
$$CO_2 + H_2 \rightleftharpoons CO + H_2O \tag{2.19}$$
$$CO_2 + 3H_2 \rightleftharpoons CH_4 + 2H_2O \tag{2.20}$$

Where equation 2.18 is the methanol synthesis reaction with $\Delta G(25\ ^\circ C) = -0.47$ kJ mol^{-1} and $\Delta H(25\ ^\circ C) = -49.5$ kJ mol^{-1} , equation 2.19 is the reverse water-gas shift (RWGS) reaction with $\Delta G(25\ ^\circ C) = 23.4$ kJ mol^{-1} and $\Delta H(25\ ^\circ C) = 41.2$ kJ mol^{-1}, and equation 2.20 corresponds to the CO_2 methanation reaction with $\Delta G(25\ ^\circ C) = -130.9$ kJ mol^{-1} and $\Delta H(25\ ^\circ C) = -252.9$ kJ mol^{-1}. The RWGS and methanation reactions needs to be considered since they are significant side reactions. Thermodynamically, the methanol synthesis will be favoured by high pressure and lower temperatures, but to activate CO_2 a high temperature is needed. This means that there might be kinetic and thermodynamic limitations for the CO_2 hydrogenation to methanol.

2.2.1 Mechanism

The mechanism of CO_2 hydrogenation to methanol with In_2O_3 has been studied using density functional theory (DFT) by Ye *et al.* [11, 12]. They concluded that the oxygen vacancies that were created on the In_2O_3 aids in the heterolytic cleavage of hydrogen. Atomic hydrogen can then react with CO_2 that has adsorbed onto the catalyst surface. In short, Ye *et al.* concluded that the synthesis route is as follows:

$$CO_2 \rightarrow^* HCOO \rightarrow {}^*H_2CO \rightarrow {}^*H_3CO \rightarrow CH_3OH \tag{2.21}$$

The rate limiting step for the methanol synthesis reaction has been determined to be the hydrogenation of H_2CO to H_3CO on the In_2O_3 surface [12].

2.2.2 Kinetic model

Ghosh *et al.* [13] has developed a LHHW kinetic model for the CO_2 hydrogenation to methanol on In_2O_3. They used the following rate expressions:

$$r_{MeOH} = \frac{k_{MeOH}}{p_{H_2}^2} \cdot \frac{p_{CO_2} \cdot p_{H_2}^3 - \frac{p_{MeOH} \cdot p_{H_2O}}{K_{eq,MeOH}}}{(1 + K_{CO_2} \cdot p_{CO_2} + \sqrt{K_{H_2} \cdot p_{H_2}})^2} \tag{2.22}$$

$$r_{RWGS} = \frac{k_{RWGS}}{\sqrt{p_{H_2}}} \cdot \frac{p_{CO_2} \cdot p_{H_2} - \frac{p_{CO} \cdot p_{H_2O}}{K_{eq,RWGS}}}{(1 + K_{CO_2} \cdot p_{CO_2} + \sqrt{K_{H_2} \cdot p_{H_2}})^2} \tag{2.23}$$

$$r_{CH_4} = k_{CH_4} \sqrt{p_{CO_2}} \sqrt{p_{H_2}} \frac{1 - \frac{p_{CH_4} \cdot p_{H_2O}^2}{p_{CO_2} \cdot p_{H_2}^4 \cdot K_{eq,CH_4}}}{(1 + K_{CO_2} \cdot p_{CO_2} + \sqrt{K_{H_2} \cdot p_{H_2}})^2} \tag{2.24}$$

Ghosh *et al.* determined that the reaction constants, activation energies, adsorption constants and enthalpy of adsorption shown in table 2.1 described their experimental data well [13].

Table 2.1: Reaction constants, activation energies, adsorption constants and enthalpy of adsorption from the model developed by Ghosh *et al.* [13]. Reaction- and adsorption constants are for 300 °C.

	Value	Unit
k_{MeOH}	$6.9 \cdot 10^{-4}$	mol s^{-1} bar^{-2} kg_{cat}^{-1}
E_{MeOH}	35.7	kJ mol^{-1}
k_{RWGS}	$1.8 \cdot 10^{-4}$	mol s^{-1} $bar^{-1.5}$ kg_{cat}^{-1}
E_{RWGS}	54.5	kJ mol^{-1}
k_{CH_4}	$1.1 \cdot 10^{-4}$	mol s^{-1} bar^{-1} kg_{cat}^{-1}
E_{CH_4}	42.5	kJ mol^{-1}
K_{H_2}	0.76	bar^{-1}
ΔH_{H_2}	-12.5	kJ mol^{-1}
K_{CO_2}	0.79	bar^{-1}
ΔH_{CO_2}	-25.9	kJ mol^{-1}

2.3 Methanol to lower olefins

The zeolite part of the bifunctional catalyst transforms the methanol produced by the In_2O_3 catalyst. The reaction from methanol to olefins over a zeolite catalyst is complex and in this thesis many reactions are lumped together to create a useful kinetic model.

2.3.1 SSZ-13 and other zeolites

A zeolite is a crystalline aluminosilicate that has a tetrahedral framework structure with enclosing cavities occupied by cations and water [14]. There are many known natural zeolites and even more synthesised zeolites with no natural counterpart [14]. Zeolites have the a wide range of uses but the major part has been catalytic work being used as a solid acid for example in isomerisation and cracking [14].

The size of the pores inside the zeolite is a very important factor to selectively synthesise lower olefins [2]. Zeolites with small pore sizes such as SAPO-34 and SSZ-13 has higher selectivity of lower olefins than other zeolites since the steric hindrance the formation of larger molecules is impeded in the relatively small cavities [2]. SAPO-34 is commonly used in industrial MTO (Methanol to olefins) reaction, although Wu and Hensen [15] reports that SSZ-13 has greater a lifetime than SAPO-34 with similar selectivities. Bleken *et al.* [16] reported that SSZ-13 has higher activity than SAPO-34 at lower temperatures since it has higher acidity, while SSZ-13 suffers from more deactivation at higher temperatures. There are also reports that shows that SAPO-34 has issues with deactivation while being stored at ambient conditions [17]. With this in mind, SSZ-13 could be a more suitable zeolite to match well with In_2O_3 to produce lower olefins from CO_2 at low temperature conditions.

2.3.2 Kinetic model

Pérez-Uriarte *et al.* [18] has performed kinetic modelling of dimethyl ether (DME) to olefins over a HZSM-5 zeolite with the following reaction scheme.

$$\mathrm{DME} \xrightarrow{k_1} \mathrm{E} + \mathrm{W} \tag{2.25}$$

$$\mathrm{DME} \xrightarrow{k_1} \mathrm{P} + \mathrm{W} \tag{2.26}$$

$$\mathrm{DME} \xrightarrow{k_1} \mathrm{B} + \mathrm{W} \tag{2.27}$$

$$\mathrm{DME} + \mathrm{W} \underset{k_2'}{\overset{k_2}{\rightleftharpoons}} 2\mathrm{MeOH} \tag{2.28}$$

$$\mathrm{MeOH} \xrightarrow{k_3} \mathrm{E} + \mathrm{W} \tag{2.29}$$

$$\mathrm{MeOH} \xrightarrow{k_3} \mathrm{P} + \mathrm{W} \tag{2.30}$$

$$\mathrm{MeOH} \xrightarrow{k_3} \mathrm{B} + \mathrm{W} \tag{2.31}$$

$$\mathrm{E} + \mathrm{DME} \xrightarrow{k_4} 2\mathrm{E} + \mathrm{W} \tag{2.32}$$

$$2\mathrm{P} + 3\mathrm{DME} \xrightarrow{k_5} 3\mathrm{P} + 3\mathrm{W} \tag{2.33}$$

$$\mathrm{B} + 2\mathrm{DME} \xrightarrow{k_6} 2\mathrm{B} + 4\mathrm{W} \tag{2.34}$$

$$\mathrm{E} + 2\mathrm{MeOH} \xrightarrow{k_7} 2\mathrm{E} + 2\mathrm{W} \tag{2.35}$$

$$\mathrm{P} + 3\mathrm{MeOH} \xrightarrow{k_8} 2\mathrm{P} + 3\mathrm{W} \tag{2.36}$$

$$\mathrm{B} + 4\mathrm{MeOH} \xrightarrow{k_9} 2\mathrm{B} + 4\mathrm{W} \tag{2.37}$$

Where MeOH is methanol, DME is dimethyl ether, E is ethylene, P is propylene, B is butylene and W is water. The model that Pérez-Uriarte *et al.* used also has some reaction for higher hydrocarbons and methane formation from DME. Pérez-Uriarte *et al.* concluded that the inhibition term was $1 + K_{MeOH} \cdot (p_{MeOH} + p_{H_2O})$.

2.3.3 Mechanism

The formation of the initial C-C bond is not completely understood and there are many different suggestions regarding the exact mechanisms [19, 20]. The formation of olefins after the first C-C bond can occur through either one of the two mechanistic pathways: One is the dual cycle mechanism where the methylation of various aliphatic compound is created in series: Methylation of ethylene yields propylene and methylation of propylene yields butylene [21]. C_6 olefins can be cycled and form aromatic hydrocarbons [21]. The other type is called the "hydrocarbon pool" (HCP), which is a pool of adsorbates represented as $(CH_x)_n$ $(0 < x < 2)$, which is then cracked to generate products such as ethylene, propylene and butylene [22]. The hydrocarbon pool may in some cases build up too much, which will fill the zeolite framework and block access for reactants [22]. Coke formation is a common issue for zeolites and causes deactivation [2]. It has been shown that only a small fraction of the ethylene and the propylene is formed by the first mechanisms [22]. In summary, the mechanism consists of two cycles: One for olefins with methylation and cracking and one for aromatics with methylation and dealkylation [23]. The rate determining step of this process is considered to be the methylation steps [2].

2.4 In_2O_3/SSZ-13 bifunctional catalyst

As mentioned, a bifunctional catalyst consisting of In_2O_3 and the zeolite SSZ-13 mixed with a specific mass ratio was used. As of May 2021, no other literature has been reported using this specific catalyst combination for the synthesis of lower olefins directly from CO_2. There are some studies with other zeolites combined with In_2O_3.

The mass ratio of In_2O_3 and SSZ-13 zeolite is an important parameter to consider along with the method for mixing the two catalysts together in order to optimise the proximity between the In_2O_3 and the zeolite. Numpilai *et al.* [6] has performed activity tests on a bifunctional In_2O_3/SAPO-34 catalysts at different operating conditions, most notably over different mass ratios of oxide to zeolite. They found that the selectivity to lower olefins was the highest with a 2:1 ratio of In_2O_3 to SAPO-34. Gao *et al.* [24, 25] also observed that highest conversion was achieved with a 2:1 In_2O_3:Zeolite ratio as well.

How the catalysts are integrated with each other plays a crucial role on the performance of the catalyst. Several studies of this using different metal oxides and zeolite has been made using mainly three different techniques [24–28]:

1. Dual bed mode in which the metal oxide and zeolite is positioned is series without mixing and separated with quartz sand.
2. Granule mixing in which both catalyst are in 200-500 μm and then mixed.
3. Mortar mixing in which particles are grounded using agate and mortar to a size of 0.5-1 μm and then mixed to increase their proximity.

When the catalysts were at very close proximity, as in mortar mixing, the selectivity of hydrocarbons was found the be the poorest [24–28]. It appears that the very

close proximity deactivates the zeolite as well as decrease the number of active sites for methanol synthesis. Highest selectivity was observed when granule mixing was used, which is believed to be due to that the equilibrium limited methanol synthesis was benefited as the methanol could migrate from the metal oxide to the zeolite in a timely fashion to convert to hydrocarbons [25]. This would then shift the equilibrium of the methanol synthesis favourably and also suppress the undesired RWGS reaction [25]. Less CO formation has been observed when granule mixing was applied, indicating that the RWGS reaction was suppressed [25]. As for the dual bed mode, it was not as good as granule mixing due to the synergistic effect of the methanol intermediates reaction quickly not being present when the catalysts are segregated [25].

3
Methods

The main work done in this thesis is the gathering of experimental data of an already synthesised In_2O_3/SSZ-13 bifunctional catalyst and to develop a kinetic model for the catalyst. The synthesis and characterisation of the catalyst are included but were not performed by the author. Those parts needs to be included as they are an important part of the work, but was not within the scope of the thesis. The methods for testing the catalytic activity as well as the modelling is also covered in this chapter. In addition to the work presented in this section, a model including mass transfer was also developed, which is presented in appendix C.

3.1 Experimental work

Experimental work done in this thesis is the activity tests of the catalysts. The catalysts synthesis and characterisation is also described as it is a vital part of the work, but has not been performed by the author of the thesis.

3.1.1 Catalyst synthesis

In_2O_3 was synthesised with a precipitation method based on the paper by Frei *et al.* [29]. Aqueous Na_2CO_3 (10 g, Sigma Aldrich, $\geq$ 99.5%) was added slowly to an aqueous solution of Indium (III) nitrate hydrate (7.7 g, Sigma Aldrich, 99.99%) that was stirred continuously until the pH was 9.2. Then the resulting solution was aged for 1 h while continuously stirred. After ageing, the solution was filtered and washed with deionized water three times and then dried in a vacuum at 50 °C overnight. The white powder of $In(OH)_3$ was then calcinated at 300 °C for 3 hours with a ramp rate of 2 °C min^{-1} to obtain crystalline In_2O_3.

SSZ-13 was made according to the following procedure by Li *et al.* [30]. N,N,N-trimethyl-1-adamantanammonium hydroxide (TMAdOH) was dissolved with NaOH and deionized water and then SiO_2 was added. Lastly Al_2O_3 was also dissolved into the mixture and then the resulting gel was stirred in ambient temperature conditions for 1 h. A gel with the compositions $0.1Na_2O : 1SiO_2 : 0.025\ Al_2O_3 : 0.2$TMAdOH : $44H_2O$ was created. After the gel was stirred it was put into a Teflon-lined container and put inside an oven at 160 °C for 6 days while being stirred continuously. Then the product was filtrated and washed with deionised water and then dried at 110 °C. After drying the catalyst was calcinated in air at 550 °C to remove the organic template. Then the excess sodium ions was removed by twice performing an ion

exchange with a 1 M NH_4NO_3 solution at 80 °C with a liquid to solid ratio of 10:1 for 3 hours. Lastly the product was calcined for 8 h at 550 °C to obtain the SSZ-13 zeolite catalyst.

After both catalysts were synthesised they were pressed, crushed and sieved into granules with a size range of 250 - 500 μm and then mixed together with a specific mass ratio.

3.1.2 Catalyst characterisation

In order to confirm that the catalysts has formed as intended during the synthesis, X-ray diffraction (XRD) was used. In XRD electromagnetic waves are sent in different angels and scattered on the solid catalyst surface [31]. Then intensity of the scattered electromagnetic waves is measured over different angels to produce a pattern [31]. From this pattern the geometric structural information about the solid catalyst is obtain by matching it to a reference pattern [31].

3.1.3 Catalytic activity tests

The catalytic activity test experiments were performed in a vertical high pressure fixed bed stainless steel reactor with an inner diameter of 1.27 cm and length of 21.5 cm placed inside a furnace. Approximately 1.0 g of the In_2O_3/SSZ-13 catalyst was positioned in the middle of the reactor so that the thermocouple tip is in contact with the catalytic bed. The catalyst was held in place with thin layers of quartz wool on both sides. The remainder of the reactor volume was filled with inert SiC particles (500 μm diameter).

When the reactor was installed, leak testing was performed. The leak test was done by pressurising the reactor slowly with argon while looking for leaks. When the pressure was high, hydrogen was slowly introduced so that the molar fraction of hydrogen was 2% and then a hydrogen sensor was used to search for leaks. Lastly, the reactor was pressurised to 40 bars and all flows in and out of the reactor was stopped for approximately 10 minutes. If the pressure remained high, the leak test was finished. Then the catalyst was activated in the reactor by heating the catalyst to 400 °C in an argon flow of 150 Nml min^{-1} for 1 hour. After the activation, the catalytic activity test were conducted.

The activity test were conducted by operating the reactor at a certain temperature, pressure, hydrogen flow and CO_2 flow. Reactor effluents was analysed with an on-line gas chromatograph (GC, SCION 456) using both thermal conductivity (TCD) and flame ionisation detectors (FID). When the reactor reached the desired pressure and temperature the GC was injected with gas once every 30 minutes until steady state was reached. Steady state was concluded when the size of the peaks were approximately constant. Steady state was reached usually after 1.5 hours. At the end of experiments the reactor was operated at standard conditions while analysing the reactor effluent every 30 minutes. Standard conditions were 30 bars , 300 °C,

75 Nml min^{-1} H_2 and 25 Nml min^{-1} CO_2.

3.1.4 Analysis of experiments

In order to have useful data the results the raw data from the gas chromatograph had to be recalculated. In this section the method for transferring GC data to molar fractions is covered as well as how other useful results were calculated.

3.1.4.1 Gas chromatography

The GC analysis was done by identifying all peaks for different species and integrating the peaks to find the their respective area. Then the molar fraction of a species was calculated as

$$y_i = A_p \cdot R_f. \tag{3.1}$$

Where A_p is the area of the peak and R_f is the response factor. In table 3.1 the response factor and retention time of all analysed species are listed.

Table 3.1: Response factors used to convert the GC results to molar fractions. Calibration has been done externally.

Species	Response factor ($\mu V^{-1} min^{-1}$)	Retention time (min)	Detector/Column
CO	$4.40 \cdot 10^{-6}$	0.76	TCD
CH_4	$1.40 \cdot 10^{-6}$	1.13	TCD
CO_2	$2.07 \cdot 10^{-5}$	2.36	TCD
C_2H_6	$4.40 \cdot 10^{-8}$	3.45	FID
C_2H_4	$7.01 \cdot 10^{-8}$	3.67	FID
C_3H_8	$2.22 \cdot 10^{-8}$	4.77	FID
C_3H_6	$4.69 \cdot 10^{-8}$	6.19	FID
C_4H_{10}	$2.22 \cdot 10^{-8}$	8.06	FID
C_4H_8	$3.49 \cdot 10^{-8}$	9.72	FID
C_5H_{10}	$1.73 \cdot 10^{-8}$	11.9	FID
C_5H_{12}	$3.53 \cdot 10^{-8}$	13.2	FID
MeOH	$2.35 \cdot 10^{-6}$	14.0	TCD

Water and H_2 are not measured but estimated from the amount of other species measured. Since the stream was cooled to room temperature before the sample point for the GC, adjustments of the molar fractions may be required if the estimated water mole fraction exceeds its saturation molar fraction. MeOH will not condense due to small amounts of these species in the reactor effluent.

3.1.4.2 Calculations for analysing experimental results

To analyse the results the CO_2 conversion, carbon selectivity, carbon balance and the molar fraction variances of repeated experiments. In this section the equations

of these are defined. The CO_2 conversion of each experiments was calculated as

$$X_{CO_2} = \frac{F_{CO_2,in} - F_{CO_2,out}}{F_{CO_2,in}}. \tag{3.2}$$

Where $F_{CO_2,in}$ and $F_{CO_2,out}$ are the molar flow rate of CO_2 at the inlet and outlet of the reactor. The carbon selectivity of all compounds were calculated as

$$S_i = \frac{(F_{i,out} - F_{i,in}) \cdot \chi_i}{F_{CO_2,in} - F_{CO_2,out}}. \tag{3.3}$$

Where $F_{i,in}$ and $F_{i,out}$ are the molar flow rate of specie i at the inlet and outlet of the reactor and χ_i is the number of carbon atoms in specie i. The carbon balance for an experiment was determined with the following equation:

$$C_B = \frac{\sum_i F_{i,out}\chi_i}{F_{CO_2,in}} \tag{3.4}$$

With the carbon balance defined as it is in equation 3.4 a carbon balance above 100% means that the total amount of carbon in the reactor outlet is overestimated and a carbon balance below 100% means that the total amount of carbon in the reactor outlet is underestimated. The molar fraction variance of species i for n number of repeated experiment were calculated with the following equation

$$s_i^2 = \frac{1}{n-1}\sum_{j=1}^{n}(y_{i,j} - \bar{y_i})^2 \tag{3.5}$$

Where s_i^2 is the estimated molar fraction variances, $y_{i,j}$ is the molar fraction of species i in experiment j and $\bar{y_i}$ is the mean molar fraction of specie i in all experiments.

3.2 Mathematical modelling

In order to develop a kinetic model, a reactor model must be used. In this section the reactor model is presented as well as the kinetic model. The method on how the parameters were fitted with the experimental data is also presented.

3.2.1 Reactor model

The reactor was modelled as an one-dimensional pseudo-homogeneous plug flow reactor. The following assumptions are made:

- Isothermal conditions
- Isobaric conditions
- The reactor is in steady state
- No mass transfer limitations
- Negligible axial dispersion

Isothermal conditions was observed by the thermocouple in the catalytic bed indicating the same temperature at the set furnace temperature. Isobaric conditions were confirmed by estimating the pressure drop with the Ergun equation [32]. Steady

state was ensured by the experimental procedure (see section 3.1.3) and negligible mass transfer limitations were confirmed with the Mears parameter [33] for outer mass transfer and Weisz-Prater parameter for inner mass transfer [34]. For calculation of pressure drop, Mears parameter and Weisz-Prater parameter, see appendix A. By doing a mass balance over a differential disc section of the catalyst bed, the mass balance equation is given.

$$\frac{dF_i}{dw} = \sum_{j=1}^{n} \nu_{ij} \cdot r_{j,\mathrm{In_2O_3}} \cdot w_{\mathrm{In_2O_3}} + \sum_{j=1}^{n} \nu_{ij} \cdot r_{j,\text{SSZ-13}} \cdot w_{\text{SSZ-13}} \tag{3.6}$$

Where F_i is the molar flow rate of specie i, w the total catalyst weight, $w_{\mathrm{In_2O_3}}$ the mass fraction of In_2O_3 in the catalyst, $w_{\text{SSZ-13}}$ the mass fraction of SSZ-13 in the catalyst, ν_{ij} the stoichiometric coefficient of specie i in reaction j, $r_{j,\mathrm{In_2O_3}}$ is the reaction rate of reaction j on In_2O_3 and $r_{j,\text{SSZ-13}}$ is the reaction rate of reaction j on SSZ-13. Since there are many species and reactions involved in the reaction, equation 3.6 yields a series of ordinary differential equations that are solved with the initial condition (at $w = 0$) being the reaction inlet condition.

3.2.2 Reaction kinetics

The models that Pérez-Uriarte *et al.* [18] and Ghosh *et al.* [13] have developed was added together and modified to be a starting point for a new kinetic model for methanol mediated CO_2 hydrogenation to lower olefins. The following reaction scheme in table 3.2 is the final version. The first version included DME/MeOH equilibrium and DME to hydrocarbon reaction, but as no DME was found during experiments those reactions were removed for simplicity. This does not mean that there is no DME to hydrocarbon reaction but that they react so fast that no DME can be measured. Since no DME was observed the kinetic parameters of these reaction would not be possible to estimate. The first and second version also assumed that butylene and pentylene formed the same way as ethylene and propylene, which was directly from methanol. With that it was not possible to get any good fit to the experimental data for C_4 and C_5. The kinetic study from Pérez-Uriarte *et al.* [18] was done with HZSM-5 which can has a larger pore size and can form larger olefins more easily than SSZ-13. Instead, the butylene and pentylene was considered to be formed from smaller olefins.

Table 3.2: Summary of all reactions used in the modelling.

Reaction number	Reaction	Description
1	$CO_2 + 3H_2 \rightleftharpoons CH_3OH + H_2O$	Methanol synthesis
2	$CO_2 + H_2 \rightleftharpoons CO + H_2O$	RWGS
3	$CO_2 + 4H_2 \rightleftharpoons CH_4 + 2H_2O$	Methanation
4	$2CH_3OH \longrightarrow C_2H_4 + 2H_2O$	Ethylene formation from methanol
4	$3CH_3OH \longrightarrow C_3H_6 + 3H_2O$	Propylene formation from methanol
5	$C_2H_4 + 2CH_3OH \longrightarrow 2C_2H_4 + 2H_2O$	Autocatalytic growth of ethylene
6	$C_3H_6 + 3CH_3OH \longrightarrow 2C_3H_6 + 3H_2O$	Autocatalytic growth of propylene
7	$C_2H_4 + H_2 \longrightarrow C_2H_6$	Ethylene hydrogenation to ethane
7	$C_3H_6 + H_2 \longrightarrow C_3H_8$	Propylene hydrogenation to propane
7	$C_4H_8 + H_2 \longrightarrow C_4H_{10}$	Butylene hydrogenation to butane
7	$C_5H_{10} + H_2 \longrightarrow C_5H_{12}$	Pentylene hydrogenation to pentane
8	$C_2H_4 \longrightarrow \frac{1}{2}C_4H_8$	Butylene formation from ethylene
8	$C_3H_6 \longrightarrow \frac{3}{4}C_4H_8$	Butylene formation from propylene
9	$C_2H_4 \longrightarrow \frac{2}{5}C_5H_{10}$	Pentylene formation from ethylene
9	$C_3H_6 \longrightarrow \frac{3}{5}C_5H_{10}$	Pentylene formation from propylene

A lumped type kinetic model was considered for the formation of olefins and paraffins as well as the autocatalytic growth of ethylene and propylene. Formation of ethylene and propylene from methanol is lumped since they have identical rate determining steps. The same is true for hydrogenation of all olefins, formation of butylene from smaller olefins and formation of pentylene from smaller olefins.The rate equations considered using LHHW kinetics are:

$$r_1 = \frac{k_1}{p_{H_2}^2} \cdot \frac{p_{CO_2} \cdot p_{H_2}^3 - \frac{p_{MeOH} \cdot p_{H_2O}}{K_{eq,1}}}{I_{In_2O_3}}, \tag{3.7}$$

$$r_2 = \frac{k_2}{\sqrt{p_{H_2}}} \cdot \frac{p_{CO_2} \cdot p_{H_2} - \frac{p_{CO} \cdot p_{H_2O}}{K_{eq,2}}}{I_{In_2O_3}}, \tag{3.8}$$

$$r_3 = k_3 \sqrt{p_{CO_2}} \sqrt{p_{H_2}} \frac{1 - \frac{p_{CH_4} \cdot p_{H_2O}^2}{p_{CO_2} \cdot p_{H_2}^4 \cdot K_{eq,3}}}{I_{In_2O_3}}, \tag{3.9}$$

$$r_4 = k_4 \frac{p_{MeOH}}{I_{\text{SSZ-13}}}, \tag{3.10}$$

$$r_5 = k_5 \frac{p_{MeOH} \cdot p_{C_2H_4}}{I_{\text{SSZ-13}}}, \tag{3.11}$$

$$r_6 = k_6 \frac{p_{MeOH} \cdot p_{C_3H_6}}{I_{\text{SSZ-13}}}, \tag{3.12}$$

$$r_7 = k_7 \frac{p_{C_2H_4/C_3H_6/C_4H_8/C_5H_{10}} \cdot p_{H_2}}{I_{\text{SSZ-13}}} \cdot f_c, \tag{3.13}$$

$$r_8 = k_8 \frac{p_{C_2H_4/C_3H_6}}{I_{\text{SSZ-13}}}, \tag{3.14}$$

$$r_9 = k_9 \frac{p_{C_2H_4/C_3H_6}}{I_{\text{SSZ-13}}}. \tag{3.15}$$

Where p_i is the partial pressure of specie i, f_c is an empirical constant, k_j is the rate constant of the reaction j and $K_{eq,j}$ is the thermodynamic equilibrium constant for reaction j. In reaction 7, the partial pressure differs depending on the species being hydrogenated while the reaction rate constant is the same regardless of species. Same is the case for reaction 8 and 9. CO_2 and H_2 are considered to adsorb onto the In_2O_3 catalyst where H_2 adsorbs dissociatively and methanol and water are considered to adsorb onto the zeolite surface. This makes the inhibition terms $I_{In_2O_3}$ and $I_{\text{SSZ-13}}$ the following:

$$I_{In_2O_3} = (1 + K_{CO_2} \cdot p_{CO_2} + \sqrt{K_{H_2} \cdot p_{H_2}})^2 \tag{3.16}$$

$$I_{\text{SSZ-13}} = 1 + K_{MeOH/H_2O} \cdot (p_{MeOH} + p_{H_2O}), \tag{3.17}$$

where K_i is the adsorption/desorption equilibrium of constant of specie i.

3.2.3 Parameter optimisation

The optimisation of the parameters in the model was done by minimising the residual sum of squares (SSR).

$$SSR = \sum_i \sum_j w_i \left(y_{i,j}^{exp} - y_{i,j}^{sim} \right)^2 \tag{3.18}$$

Where w_i is a weighing factor for specie i, $y_{i,j}^{exp}$ is the experimental mole fraction of specie i and experiment j and $y_{i,j}^{sim}$ is the corresponding mole fraction estimated

from equation 3.6, which was calculated using the ode15s solver in Matlab R2019b (Mathworks, Inc.). The parameters tuned to minimise SSR comes from the rate constants and the adsorption equilibrium constants [7].

$$k_j = k_{j,ref} \cdot exp\left(\frac{E_j}{R}\left(\frac{1}{T_{ref}} - \frac{1}{T}\right)\right) \tag{3.19}$$

$$K_i = K_{i,ref} \cdot exp\left(\frac{\Delta H_i}{R}\left(\frac{1}{T_{ref}} - \frac{1}{T}\right)\right) \tag{3.20}$$

Where $k_{j,ref}$ is the rate constant at the reference temperature T_{ref}, E_j is the activation energy, $K_{i,ref}$ is the adsorption equilibrium constant at the reference temperature, ΔH_i is the enthalpy change of adsorption and R is the gas constant. Equation 3.19 is called the reparameterised Arrhenius equation and equation 3.20 is the reparameterised Van't Hoff equation. These equations are reparameterised in order to minimise the correlation between the pre-exponential factor with the parameter in the exponent (activation energy or enthalpy change). The reference temperature for all equations is the same temperature as in the standard condition in the experiments.

The hydrogenation of ethylene, propylene and butylene were assumed to have the same rate constant as the mechanism are the same and therefore the temperature dependency on the reaction should be the same. But the consumption is not exactly the same. Therefore, one consumption factor which describes the relative consumption of ethylene, butylene and pentylene with reference to propylene was also tuned. Minimisation of SSR was done by non-linear regression using the 'lsqnonlin' subroutine, which is based on the Levenberg-Marquardt method, in Matlab optimisation package. The solver utilises gradient based optimisation with SSR as the objective function.

3.2.4 Analysis of the model

In order to quantify the model performance and sensitivity the R^2 value and the normalised sensitivity coefficients (S) were calculated. The R^2 value was calculated as

$$R^2 = 1 - \frac{\sum_i \sum_j w_i \left(y_{i,j}^{exp} - y_{i,j}^{sim}\right)^2}{\sum_i \sum_j w_i \left(y_{i,j}^{exp} - \bar{y_i}^{exp}\right)^2} \tag{3.21}$$

Where $\bar{y_i}^{exp}$ is the average molar fraction from all experiments of specie i. The R^2 value is the fraction of all variance in the experiments the model can predict. The normalised sensitivity coefficients for each parameter was calculated as [13]

$$S = \beta_0 \frac{\sum_i \left(\frac{\Delta y^{sim}}{y_0^{sim}}\right)^2}{\Delta\beta}, \tag{3.22}$$

where β_0 is the parameter at its optimal value, $\Delta\beta$ is the change in parameter from its optimal value, y_0^{sim} is the simulated mole fraction when the parameter is at its optimal value and Δy^{sim} is the the change in simulated mole fraction when the parameter is changed from its optimal value. The normalised sensitivity coefficients evaluates each parameters effect on the simulations output. A parameter with a relatively large sensitivity coefficient means that the parameter could be more accurately estimated from the data. But as the sensitivity coefficient is a relative measurement there is no absolute value that should be achieved. In this paper all normalised sensitivity coefficients are calculated with a 0.1% change in the parameter value. Residuals are also calculated to analyse the model, which are the difference between the simulated molar fraction and the experimentally determined molar fraction and is defined as

$$e_i = y_i^{sim} - y_i^{exp}. \tag{3.23}$$

Where e_i is the residual of specie i.

4

Results and discussion

Characterisation of the catalyst, catalytic activity testing and mathematical modelling are the main work of this thesis. In this chapter, the results of this work is presented and discussed.

4.1 Experimental results

In this section the results from the experimental work of catalyst characterisation and catalytic activity testing is presented and discussed.

4.1.1 Catalyst characterisation

The XRD (X-Ray Diffraction) patterns for the In_2O_3 catalyst and the SSZ-13 zeolite catalyst that were used are shown in figure 4.1a and figure 4.1b.

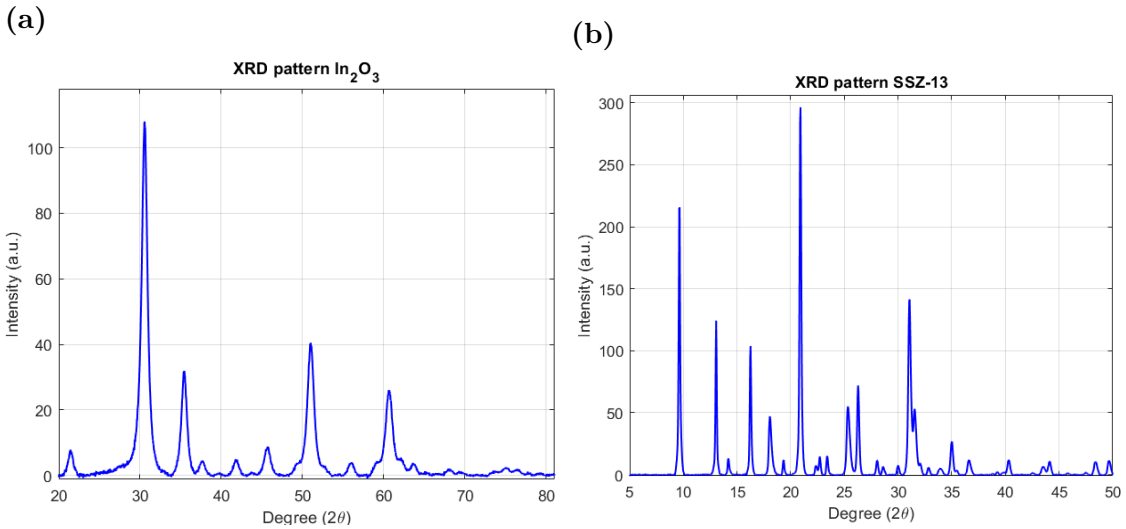


Figure 4.1: XRD patterns for In_2O_3 **(a)** and SSZ-13 zeolite **(b)**.

For the In_2O_3 the distinct peaks confirms the crystallinity of the sample. The peaks at 21.5°, 30.6°, 35.5°, 37.7°, 41.9°, 45.7°, 51.0°, 56.1°, 60,7°, 63.7°, 68.0°and 76.3°corresponds to the (2 1 1), (2 2 2), (4 0 0), (4 1 1), (3 3 2), (4 3 1), (4 4 0), (6 1 1), (6 2 2), (4 4 4), (7 2 1) and (7 4 1) planes respectively [13]. The numerous peaks for the SSZ-13 pattern corresponds to the chabazite (CHA) topology structure [30]. The

XRD results confirm that both the In_2O_3 and SSZ-13 catalysts have the crystallinity as intended.

4.1.2 Catalytic activity

To understand how the catalyst behaves at different conditions and to have a wide range of data for the model, a series of experiments was conducted. The reaction conditions for the different experiments are listed in table 4.1 and the CO_2 conversion and carbon selectivities of these experiments are listed in table 4.2.

Table 4.1: Experimental conditions for the different experiments conducted.

Exp.	**P (bar)**	**T (°C)**	**WHSV (Nml $g_{cat}^{-1}h^{-1}$)**	**H_2:CO_2**
1a	30	400	6000	3:1
1b	30	375	6000	3:1
1c	30	350	6000	3:1
1d	30	325	6000	3:1
1e	30	300	6000	3:1
1f	30	275	6000	3:1
1g	30	250	6000	3:1
2a	20	300	6000	3:1
2b	30	300	6000	3:1
2c	40	300	6000	3:1
3a	30	300	6000	2:1
3b	30	300	6000	3:1
3c	30	300	6000	4:1
4a	30	300	3000	3:1
4b	30	300	4000	3:1
4c	30	300	6000	3:1
4d	30	300	8000	3:1
5a	30	362	6000	3:1
5b	30	337	6000	3:1
5c	30	312	6000	3:1
5d	30	287	6000	3:1
5e	25	300	6000	3:1
5f	35	300	6000	3:1

No DME was found during any experiment and only very small amounts of C_{6+} in some experiments. In addition to the experiments listed in table 4.1, a series of experiments were conducted at standard conditions to monitor the stability of the catalyst and to check whether any catalyst deactivation occurs. The standard conditions considered is a pressure at 30 bar, a temperature at 300 °C, a WHSV at 6000 Nml $g_{cat}^{-1}h^{-1}$ and a H_2:CO_2 of 3:1. Experiments 1a to 4d was done in the same week and experiments 5a to 5f was done two weeks after the first set of experiments. The reactor was operated at 400 °C for 1 h in the beginning of each day in order remove

any possible coke deposition on the catalyst. Some of the results are presented in appendix B.1 as they were of lesser interest.

Experiments 1a to 1e were performed twice due the observation that the catalytic activity was low initially and increased after some time. The reason for this could be that the hydrocarbon pool needed some time to build up on the zeolite. In experiments 1a to 1g and 5a to 5d the reactor temperature was varied, in experiments 2a, 2b, 2c, 5e and 5f the total reactor pressure was varied, in experiments 3a, 3b and 3c the H_2:CO_2 ratio was varied and in experiments 4a, 4b, 4c and 4d the WHSV was varied. Experiments 5a to 5f were complementary experiments done two weeks after the first set of experiments. Note that experiments 1e, 2b, 3b and 4c are repetitions of the standard reactor conditions.

Table 4.2: CO_2 conversion, carbon selectivity and carbon balance for all experiments calculated with equation 3.3, equation 3.2 and equation 3.4 respectively. HC stands for hydrcocarbons, Ol stands for olefins, Pf stands for paraffins and C_B is the carbon balance.

Exp.	$\mathbf{X}_{CO_2}$ (%)	$\mathbf{S}_{MeOH}$ (%)	$\mathbf{S}_{CO}$ (%)	$\mathbf{S}_{CH_4}$ (%)	$\mathbf{S}_{HC}$ (%)	$\mathbf{S}_{Ol}$ (%)	$\mathbf{S}_{Pf}$ (%)	$\mathbf{C}_B$ (%)
1a	22.2	0.0	68.4	0.9	30.7	9.7	22.0	91.5
1b	16.3	0.0	61.7	1.0	37.3	16.5	21.8	100.8
1c	11.3	2.3	51.2	2.0	44.5	30.3	16.2	109.5
1d	6.5	14.5	41.4	1.9	42.2	35.3	8.8	114.3
1e	3.4	11.3	38.0	1.4	49.4	42.2	8.6	119.6
1f	1.7	35.4	40.9	1.1	22.6	19.7	3.9	119.5
1g	0.5	71.2	9.5	0.7	18.5	16.0	3.2	123.1
2a	3.0	18.8	39.7	1.2	40.4	35.6	5.9	121.0
2b	3.8	14.6	32.6	1.0	51.8	42.9	9.8	117.8
2c	3.6	15.3	36.5	1.6	46.6	39.4	8.8	120.2
3a	2.4	25.9	40.9	1.4	31.8	27.5	5.6	126.1
3b	3.3	21.8	37.8	1.5	38.9	33.1	7.2	117.7
3c	4.0	11.7	37.0	1.4	49.8	41.3	10.0	117.1
4a	3.6	0.0	40.2	1.2	58.6	43.2	16.6	114.3
4b	3.5	11.5	40.2	1.6	46.6	38.2	10.1	115.8
4c	3.2	32.2	36.4	1.4	30.0	25.4	6.0	118.9
4d	2.8	38.9	38.4	1.4	21.4	18.3	4.5	123.1
5a	13.5	0.0	55.9	1.1	43.0	23.5	20.7	108.7
5b	8.4	5.0	45.0	1.9	48.1	36.6	13.4	116.9
5c	4.0	30.2	40.8	1.8	27.2	21.9	7.1	121.1
5d	2.0	27.7	41.4	1.2	29.7	24.7	6.2	119.6
5e	3.6	44.5	32.7	1.3	21.5	17.9	4.8	120.1
5f	2.7	33.6	44.3	1.9	20.3	16.6	5.5	122.5

In general there are some non-random experimental errors which can be caused by things such as:

- Steady state not being reached
- Poor calibration of GC
- Catalyst deactivation
- Human errors

Steady state not being reached and human errors should be avoided if everything has been done correctly and there were no signs of these errors. As for the calibration of the GC it was not done by the author and the calibration should be assumed to be okay unless there are signs that it is not good. As the carbon balance is larger than 100% for most experiments there are signs that one or more species has been overestimated. It is most likely the CO_2 due to reasons discussed in section 4.2.2. Catalyst deactivation can be difficult to avoid with some catalyst. During these experiments, there was sign of it when the reactor was operated at low temperatures for long times. Therefore, the experiments were done such that the low temperature experiments were done at the end of the day and the catalyst was always exposed to high temperatures between days as it recovered the catalyst activity. With that in mind, the experiment at lower temperatures should not be trusted as much as those done at higher temperatures.

Random errors in the experiments can be from things as small variation in reactor conditions such as flow-, temperature- and pressure variations and variations in GC measurements. Since experiments 1e, 2b, 3b and 4c are repeats of the same reactor conditions the variance of the measured molar fractions of each specie can be estimated. In table 4.3 the estimated variance of the measured molar fractions are presented. By assuming that the variance is constant for all conditions, it is possible to use the estimated variance to see if the kinetic model can make the prediction within the experimental variance. If the model can do that it can be assumed that there is no significant lack of fit for the model.

Table 4.3: Molar fraction variance of different species measured as defined in equation 3.5. H_2, DME and water are not measured and therefore not included.

Specie	**Variance**
CO_2	$6.13 \cdot 10^{-6}$
MeOH	$4.89 \cdot 10^{-7}$
CO	$1.66 \cdot 10^{-8}$
CH_4	$1.72 \cdot 10^{-10}$
C_2H_4	$9.98 \cdot 10^{-9}$
C_2H_6	$5.55 \cdot 10^{-12}$
C_3H_6	$1.79 \cdot 10^{-8}$
C_3H_8	$3.23 \cdot 10^{-9}$
C_4H_8	$3.76 \cdot 10^{-9}$
C_4H_{10}	$6.19 \cdot 10^{-11}$
C_5H_{10}	$1.28 \cdot 10^{-10}$
C_5H_{12}	$5.71 \cdot 10^{-13}$

4.1.2.1 The influence of temperature on catalytic activity

In figure 4.2 the carbon selectivities and CO_2 conversion over different reactor temperatures are shown.

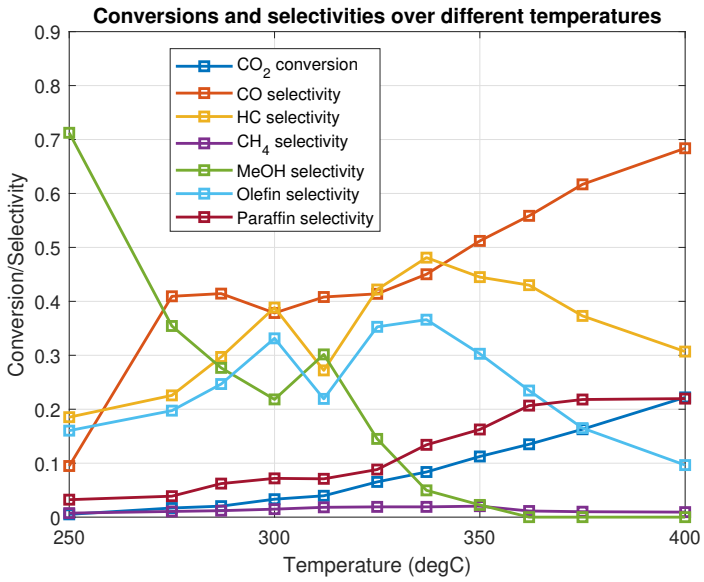


Figure 4.2: Carbon selectivities and CO_2 conversion calculated with equation 3.3 and equation 3.2 respectively over different reactor temperatures. Experiments included are 1a to 1g and 5a to 5d.

Figure 4.2 shows that the CO_2 conversion, CO selectivity and paraffin selectivity increases with increasing temperature while the rest decreases with temperature. The increased CO_2 conversion is expected due to the increased CO_2 activation when the temperature increases. The CO selectivity is high at high temperatures due to it being thermodynamically favoured at high temperature as RWGS is an endothermic reaction. The methanol selectivity is the highest at low temperatures which is consistent with the thermodynamics of the reactions occurring on the In_2O_3 surface (MeOH synthesis, RWGS and methanation). At high temperatures there is no trace of methanol since it reacts fast to olefins. In figure 4.2 there is a significant deviation at 312 °C, which is likely due to deactivation of the zeolite. The fact that the methanol is higher than expected, all hydrocarbons are lower than expected and CO and CH_4 is not deviated suggest that the SSZ-13 catalyst has deactivated somewhat in that experiment.

The increase in paraffin selectivity at high temperatures is likely due to the hydrogenation reactions becoming more dominant at higher temperatures than the olefins producing reactions, which would also be a cause of lowered olefin selectivity at higher temperatures. The overall decrease in hydrocarbon selectivity is due to the RWGS reaction becoming rapid and not that the reaction rates for producing hydrocarbons decreases.

When comparing the CO selectivity with the same amount of pure In_2O_3 catalyst (0.67 g) from Ghosh *et al.* [13] it has higher selectivity at high temperatures and lower selectivities at low temperatures. The reason for the higher selectivities at low temperatures is likely deactivation but the reason for the lower selectivities at high temperatures are consistent with what has been reported for this type of bifunctional catalyst [25]. The suppression of the RGWS reaction leads to lower CO selectivity which is caused by the normally equilibrium limited methanol reaction having less equilibrium related limitation due to the further reaction of methanol to hydrocarbons. From the results that Ghosh *et al.* [13] presented it was concluded that the methanol synthesis was equilibrium limited at high temperatures and at 400 °C had a selectivity of 1.25% while this catalyst had a carbon selectivity of 30.7% at 400 °C (a comparable condition). This means that using a bifunctional catalyst for methanol mediated CO_2 hydrogenation can circumvent the equilibrium limitations that methanol synthesis has.

It is of interest to see what kind of hydrocarbons that are produced in the catalyst and how the reactor conditions change that. In figure 4.3 the distribution over different temperatures of all hydrocarbons measured is shown.

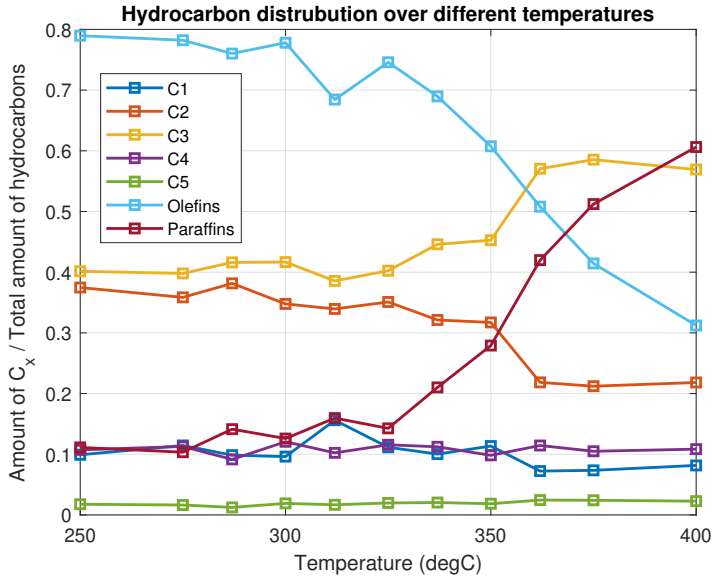


Figure 4.3: Molar based hydrocarbon distribution over different temperatures. Note that CH_4 is not included among paraffins. Experiments included are 1a to 1g and 5a to 5d.

For the most part the hydrocarbon distribution is fairly constant over the different temperature where there is 42% C_3, 34% C_2, 13% C_4, 8% C_1 and 2% C_5. The only significant temperature effect that the C_3 increases and C_2 decreases significantly at high temperatures. The distribution of olefins is the highest at lower temperatures and lowest at higher temperatures where the paraffins are most numerous. This suggest that the hydrogenation of olefins are significant reactions at high temperatures, which is something that can also be read from figure 4.2.

4.1.2.2 The influence of residence time on catalytic activity

The CO_2 conversion and carbon selectivities over different weight hourly space velocity, which is inversely proportional to the mean residence time of the reactor, is shown in figure 4.4. In figure 4.5 the distribution of hydrocarbons over different WHSV is shown.

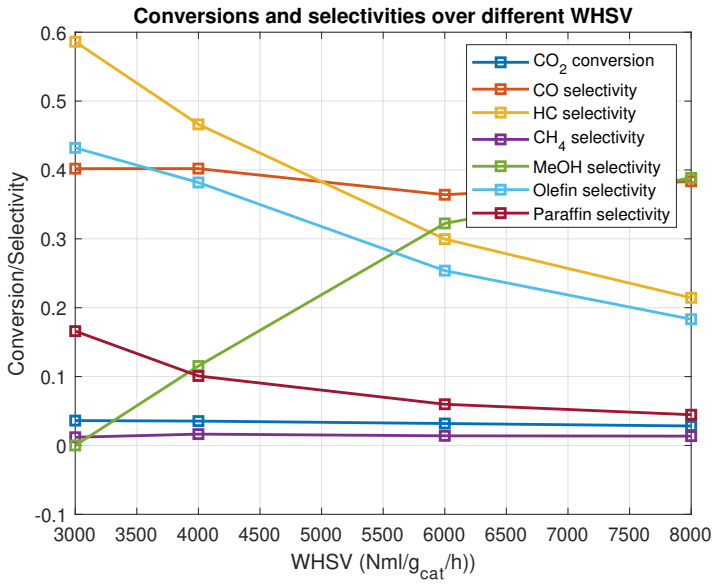


Figure 4.4: Carbon selectivities and CO_2 conversion calculated with equation 3.3 and equation 3.2 respectively over different weight hourly space velocity. Experiments included are 4a, 4b, 4c and 4d.

Figure 4.4 shows that the olefin- and paraffin selectivity decreases with increased WHSV and that CO and CH_4 selectivity is mostly unaffected by residence time. A higher selectivity of hydrocarbons is expected when the residence time is larger due to the autocatalytic reactions that produce more hydrocarbons and that the hydrocarbons is formed via methanol in series. It can also be seen that the methanol selectivity decreases rapidly as the residence time increases.

At high residence times (low WHSV) the larger hydrocarbons C_3, C_4 and C_5 are increasing slightly while C_2 is decreasing. This is likely due to that larger olefins are formed from smaller olefins. Consequently, high residence time would mean that the amount of higher hydrocarbons should increase, which can be seen in figure 4.5. Olefin selectivity is the lowest at 3000 and at 8000 Nml g_{cat}^{-1} min^{-1} and highest somewhere in between. At low WHSV the reason for low olefin selectivity is likely to be the hydrogenation of olefins as the paraffins increases at low WHSV. At high WHSV the low olefin selectivity is likely due to the methanation reaction being more prominent, which may be due to methanation not having as many intermediate steps as the production of other hydrocarbons.

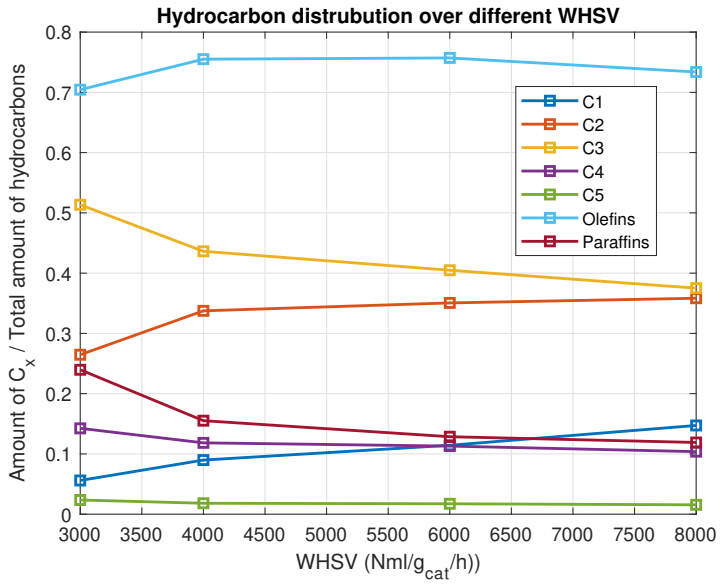


Figure 4.5: Molar based hydrocarbon distribution over different WHSV. Note that CH_4 is not included among paraffins. Experiments included are 4a, 4b, 4c and 4d.

4.1.2.3 The influence of H_2:CO_2 ratio on catalytic activity

Different inlet molar ratios of CO_2 and H_2 were also tested. A plot over different carbon selectivities and CO_2 conversion is shown in figure 4.6.

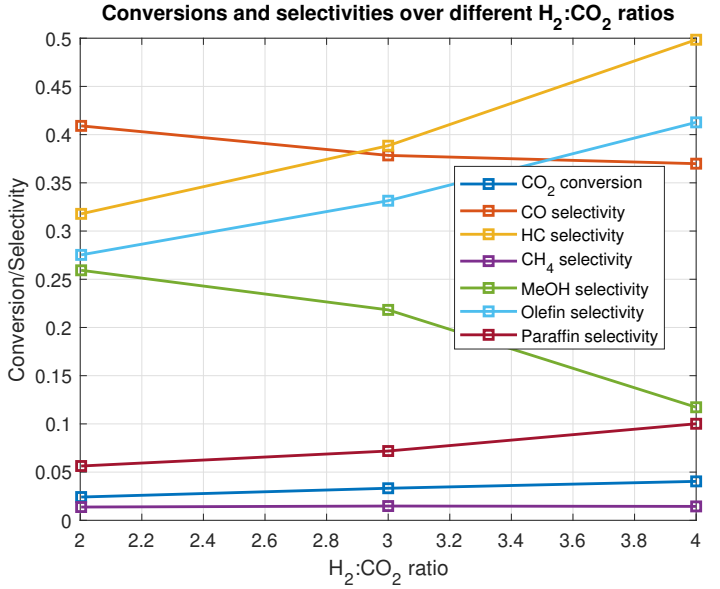


Figure 4.6: Carbon selectivities and CO_2 conversion calculated with equation 3.3 and equation 3.2 respectively over different H_2:CO_2 ratios. Experiments included are 3a, 3b and 3c.

Increased H_2:CO_2 ratio leads to increased selectivity of olefins and paraffins and

decreased selectivity of CO and methanol. CO_2 conversion is also the highest at high H_2:CO_2 ratio. It has been shown that the methanol synthesis increases with increasing H_2:CO_2 ratio when using a pure In_2O_3 as the catalyst [13], which would explain the increased olefin and paraffin selectivities. What is not explained in this study is why the methanol selectivity decreases with increased H_2:CO_2 ratio. The reactions rate expression where the reaction is consuming methanol from section 3.2.2 are independent of H_2 partial pressure. The cause may be that the autocatalytic reactions are consuming methanol. So if there is more methanol produced there is more olefins and therefore more autocatalytic reactions, which consumes methanol. What remains to be seen is that if the model is able to predict this trend or not. An experimental error could also give rise to this effect and could for example be that the flow of H_2 and CO_2 into the reactors are not correct, which could lead to flow not being a total of 100 Nml/min as it should be. It is more likely that there is some unknown effect that involves H_2 that is the cause of the methanol selectivity decreasing with higer H_2:CO_2 ratio. In figure 4.7 the distribution of hydrocarbons over different H_2:CO_2 ratios is shown. There are no significant changes in the hydrocarbon distribution over different H_2:CO_2 ratios except for very small changes in C_1, C_2 and C_3.

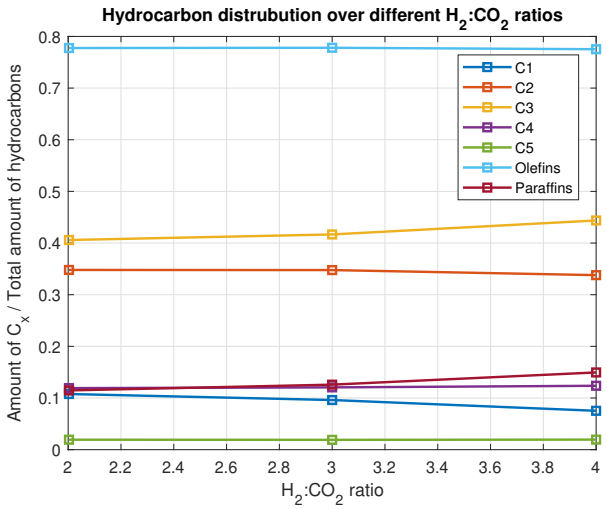


Figure 4.7: Molar based hydrocarbon distribution over different H_2:CO_2 ratios. Note that CH_4 is not included among paraffins. Experiments included are 3a, 3b and 3c.

4.1.2.4 Stability of catalyst

In order to test the stability of catalyst the reactor was operated at the standard condition (30 bars, 300 °C, 6000 Nml g_{cat}^{-1} h^{-1} for a time while the reactor effluents was frequently measured. In figure 4.8 the CO_2 conversion and carbon selectivity of some species are shown over time on stream. In figure 4.8 the extra experiments that are not listed in table 4.1 are those after 25 hours. As can be seen in figure 4.8 there seem to be a small amount of deactivation of the zeolite when the reactor is operated at standard conditions but that the procedure to bring the reactor to 400 °C regularly seems to kept the catalyst active during most experiments. Nevertheless, this is a

problem that makes the catalyst less usable in industrial application as the catalyst would need frequent reactivation. Either the reactor should be operated at higher temperature than 300 °C or that modification to the SSZ-13 zeolite should be made so that it is more stable. Even though this is a problem for the catalysts usability in industrial applications the data retrieved should still be usable for modelling.

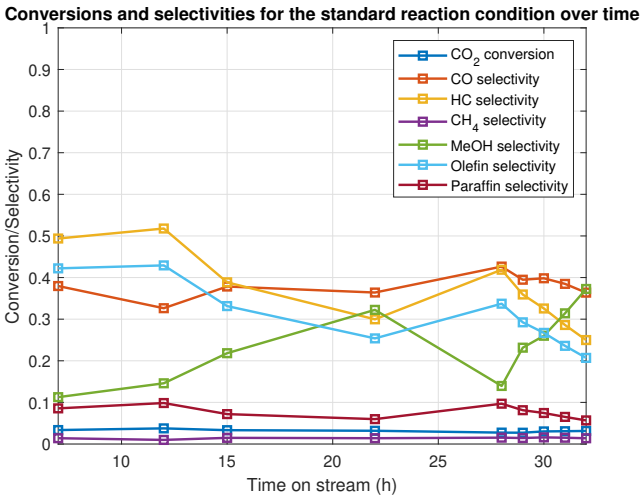


Figure 4.8: CO_2 conversion and carbon selectivities at standard reactor conditions calculated with equation 3.3 and equation 3.2 respectively over the time that the reactor was operated.

4.2 Mathematical modelling

A kinetic model has been developed such that it is able to predict the experimental data, which is presented in section 3.2. The model at its current state and with the experiments conducted has a R^2 value of 91.6%. In this section the final kinetic parameters are presented and the model is evaluated.

4.2.1 Determination of kinetic parameter values

The kinetic parameters that Ghosh *et al.* [13] determined for methanol synthesis are the same for this model and has not been changed. The In_2O_3 catalyst was the same as the one that Ghosh *et al.* used. Assuming that the catalyst does not change composition when it is physically mixed with the zeolite means that it is reasonable that the kinetic parameters from Ghosh *et al.* should apply here. The inhibition term for the zeolite that was taken from Pérez-Uriarte *et al.* [18] was also the same as the experimental data available is not useful to resolve the adsorption/desorption equilibrium in the inhibition term. In table 4.4 the reference reaction constant (at 300 °C), their unit and their normalised sensitivity coefficient are presented.

Table 4.4: Reference rate constants for the final model and their normalised sensitivity coefficient.

Reaction	k_{ref}	Unit	Normalised sensitivity
1	$6.90 \cdot 10^{-4}$	mol s^{-1} bar^{-2} kg_{cat}^{-1}	$1.08 \cdot 10^{-1}$
2	$1.80 \cdot 10^{-3}$	mol s^{-1} $bar^{-1.5}$ kg_{cat}^{-1}	$4.38 \cdot 10^{-2}$
3	$1.10 \cdot 10^{-4}$	mol s^{-1} bar^{-1} kg_{cat}^{-1}	$2.81 \cdot 10^{-2}$
4	$7.94 \cdot 10^{-3}$	mol s^{-1} bar^{-1} kg_{cat}^{-1}	$7.75 \cdot 10^{-2}$
5	$1.95 \cdot 10^{-1}$	mol s^{-1} bar^{-2} kg_{cat}^{-1}	$2.74 \cdot 10^{-3}$
6	$5.11 \cdot 10^{-1}$	mol s^{-1} bar^{-2} kg_{cat}^{-1}	$1.22 \cdot 10^{-2}$
7	$1.42 \cdot 10^{-3}$	mol s^{-1} bar^{-2} kg_{cat}^{-1}	$8.68 \cdot 10^{-2}$
8	$2.25 \cdot 10^{-2}$	mol s^{-1} bar^{-1} kg_{cat}^{-1}	$4.53 \cdot 10^{-2}$
9	$5.50 \cdot 10^{-3}$	mol s^{-1} bar^{-1} kg_{cat}^{-1}	$5.21 \cdot 10^{-2}$

If a parameter has a high normalised sensitivity coefficient it is an indication that the experiments were suitable for resolving the parameter. As the parameters involved in reaction 1, 2 and 3 were not changed at all from the model developed by Ghosh *et al.* [13] as it was assumed that those parameters were accurately resolved. Excluding reaction 1, 2 and 3 the normalised sensitivity coefficients were all in the same order of magnitude except for reaction 5, which was autocatalytic growth of ethylene. This suggest that the autocatalytic growth of propylene was more important than the autocatalytic growth of ethylene, which is also reflected in the relatively lower reaction rate constant. In table 4.5 the activation energies of the reaction and their normalised sensitivity coefficients are presented.

Table 4.5: Activation energies for the final model and their normalised sensitivity coefficient.

Reaction	E_a (kJ mol^{-1})	Normalised sensitivity
1	35.7	$8.18 \cdot 10^{-3}$
2	54.5	$1.76 \cdot 10^{-2}$
3	42.5	$5.52 \cdot 10^{-3}$
4	89	$3.71 \cdot 10^{-2}$
5	97	$9.99 \cdot 10^{-3}$
6	100	$1.05 \cdot 10^{-1}$
7	90	$8.68 \cdot 10^{-2}$
8	42	$8.93 \cdot 10^{-3}$
9	42	$1.00 \cdot 10^{-2}$

For the activation energies the olefin hydrogenation (reaction 6) has the largest normalised sensitivity coefficient by a factor of 10, which suggest that the activation energy was successfully resolved. The other activation energies have a normalised sensitivity coefficient of the same order of magnitude, which suggest that they were all reasonable successfully resolved. In table 4.6 the empirical constants f_c in equation 3.13 are presented

Table 4.6: The empirical factors from equation 3.13 for the final model and their normalised sensitivity coefficient.

Specie	f_c	Normalised sensitivity
C_2H_4	0.25	$2.42 \cdot 10^{-2}$
C_3H_6	1.00	-
C_4H_8	0.34	$2.31 \cdot 10^{-2}$
C_5H_{10}	0.16	$2.53 \cdot 10^{-3}$

The sensitivity coefficient for the rate constant for hydrogenation of pentylene to pentane is a order of magnitude lower than the rest. This suggests that the different experiments conducted does not resolved that parameter appropriately. As there are no obvious reason for why this empirical constant has a lower normalised sensitivity coefficient, the only way to improve the resolving of this parameter is to feed pentylene into the reactor during experiments. In table 4.7 the reference adsorption equilibrium constants and their respective heat of adsorption are presented together with their normalised sensitivity coefficient.

Table 4.7: Reference adsorption equilibrium constants and heat of adsorption for the final model and their normalised sensitivity coefficient.

Parameter	Value	Unit	Normalised sensitivity
$K_{CO_2,ref}$	0.830	bar^{-1}	$2.12 \cdot 10^{-2}$
$K_{H_2,ref}$	0.949	bar^{-1}	$2.21 \cdot 10^{-1}$
$K_{MeOH/H_2O,ref}$	12.9	bar^{-1}	$2.62 \cdot 10^{-1}$
ΔH_{CO_2}	-12.45	kJ mol^{-1}	$2.63 \cdot 10^{-4}$
ΔH_{H_2}	-25.85	kJ mol^{-1}	$7.60 \cdot 10^{-3}$
$\Delta H_{MeOH/H_2O}$	-0.2	kJ mol^{-1}	$7.88 \cdot 10^{-7}$

The parameters presented in table 4.7 are the same as that from Ghosh *et al.* and Pérez-Uriarte *et al.* produced as it was deemed difficult or unnecessary to resolve. It was very difficult to resolve the heat of adsorption values which has very low normalised sensitivity coefficients. In order to fully resolve the heat of adsorption parameters experiments varying both the partial pressure of the adsorbed species and the temperature is required. Since no feeding of methanol or water is done, the normalised sensitivity coefficient for $\Delta H_{MeOH/H_2O}$ is especially low.

4.2.2 Comparison of model predictions with experiments

A very important criterion for the kinetic model is that it is able to predict the trends of the experimental data. Unfortunately, there was no time to perform experiments with the sole purpose of validating the kinetic model. In this section the model prediction are presented and compared with the experiments to see whether the model is able predict the experimental data at varying reactor conditions.

4.2.2.1 Olefins predictions compared with experimental results

In figure 4.9 the experimental results are plotted along with the outputs of the model. The lengths of the bars in figure 4.9 corresponds to band in which the predictions are assumed to be within range of the random errors, which was calculated from the variances in table 4.3 and with p value of 95%. Note that the variances were calculated at the set standard reactor conditions and the variances at other conditions is likely to be different. Therefore, the band should be taken with a grain of salt and be a guideline comparing the relative size of the variances between the repeated experiments and all experiments.

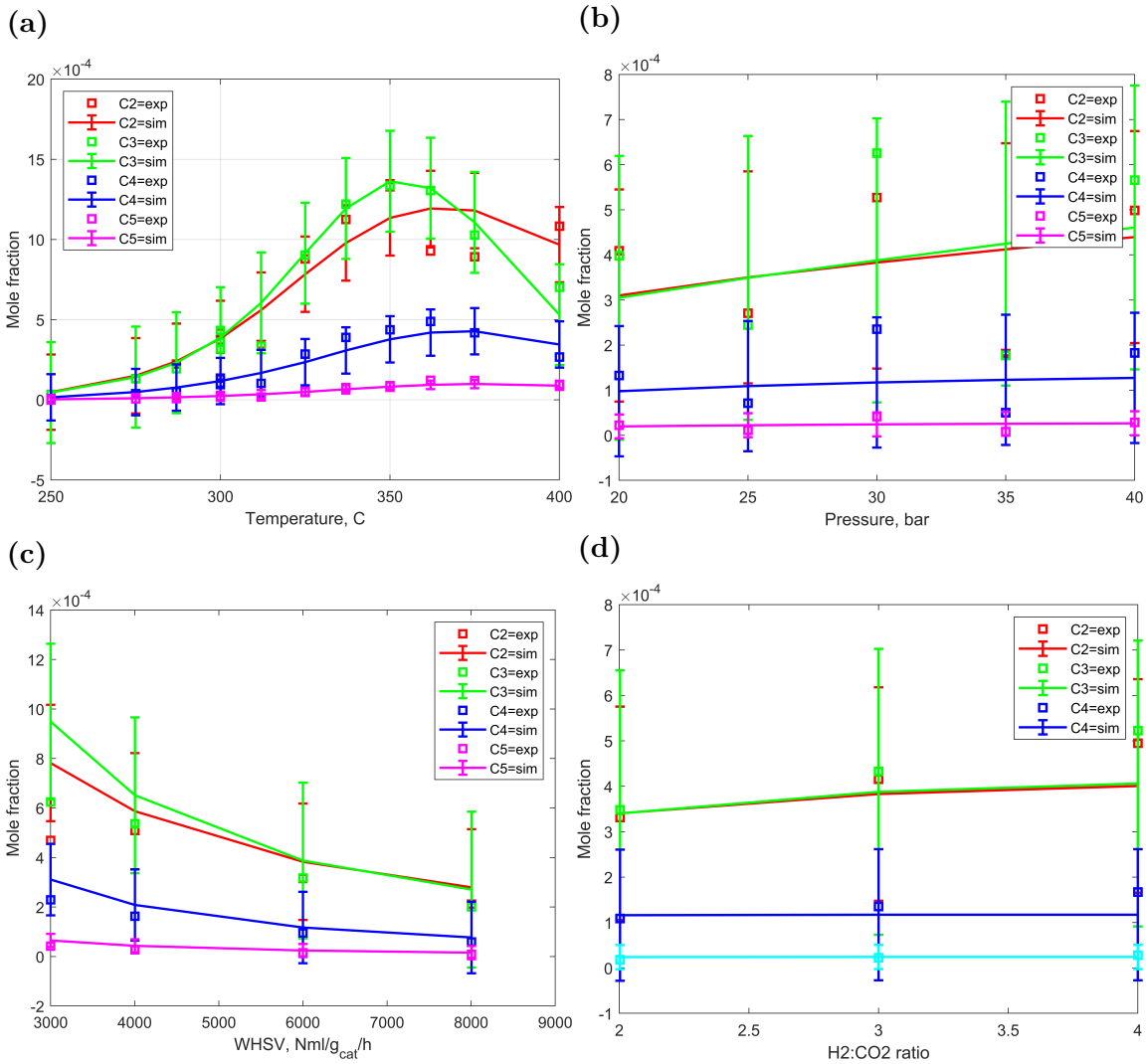


Figure 4.9: Model predictions of various olefin molar fractions compared with the experimental results for varying temperature **(a)**, total pressure **(b)**, WHSV **(c)** and H_2:CO_2 molar feed ratio **(d)**. Unless otherwise indicated conditions are 300°C, 30 bar, 6000 Nml/g/h and 3:1 H_2:CO_2 molar feed ratio.

In figure 4.9a the model predictions are compared with the experimental results over different temperatures it can be seen that the model is able to predict the

experimental data well with the exception of the ethylene prediction at high temperatures. At high temperatures the concentration of olefins generally drop, which is an effect that is both shown in the experimental data and the model. This is due to the methanol synthesis part of the reaction becoming rate limiting for the olefin production and that the olefins reacts further to paraffins to a greater extent. This is something that can be seen in the model as the olefin producing reaction have a lower activation energy than the reactions consuming olefins.

For figure 4.9b and figure 4.9d the variances of the repeated experiments are in the same magnitude as the variance between the experiments conducted with different pressures and H_2:CO_2 ratios, so it is difficult to say anything conclusive about that data. What is worth mentioning is that the trend of the model follows the same trend as the experiments. For the pressure the olefin concentration are the highest at 30 bar for the experiments but highest at 40 bar for the model, this means that it is likely some room for improvement. For example in the reaction order if the driving force term in the olefin hydrogenation reaction may be adjusted. For the H_2:CO_2 ratio the trend is the same for both the experiments and the model predictions. But both changes are small in general for both pressure and H_2:CO_2 ratio. In figure 4.9c the olefin concentration over various WHSV are shown where the model predictions follow the experimental data nicely. There is a slight over prediction of the model at low WHSV.

4.2.2.2 Paraffin predictions compared with experimental results

In figure 4.10 the model predictions of various paraffins are compared with the experimental results. The length of the bars are calculated in the same way as for figure 4.9.

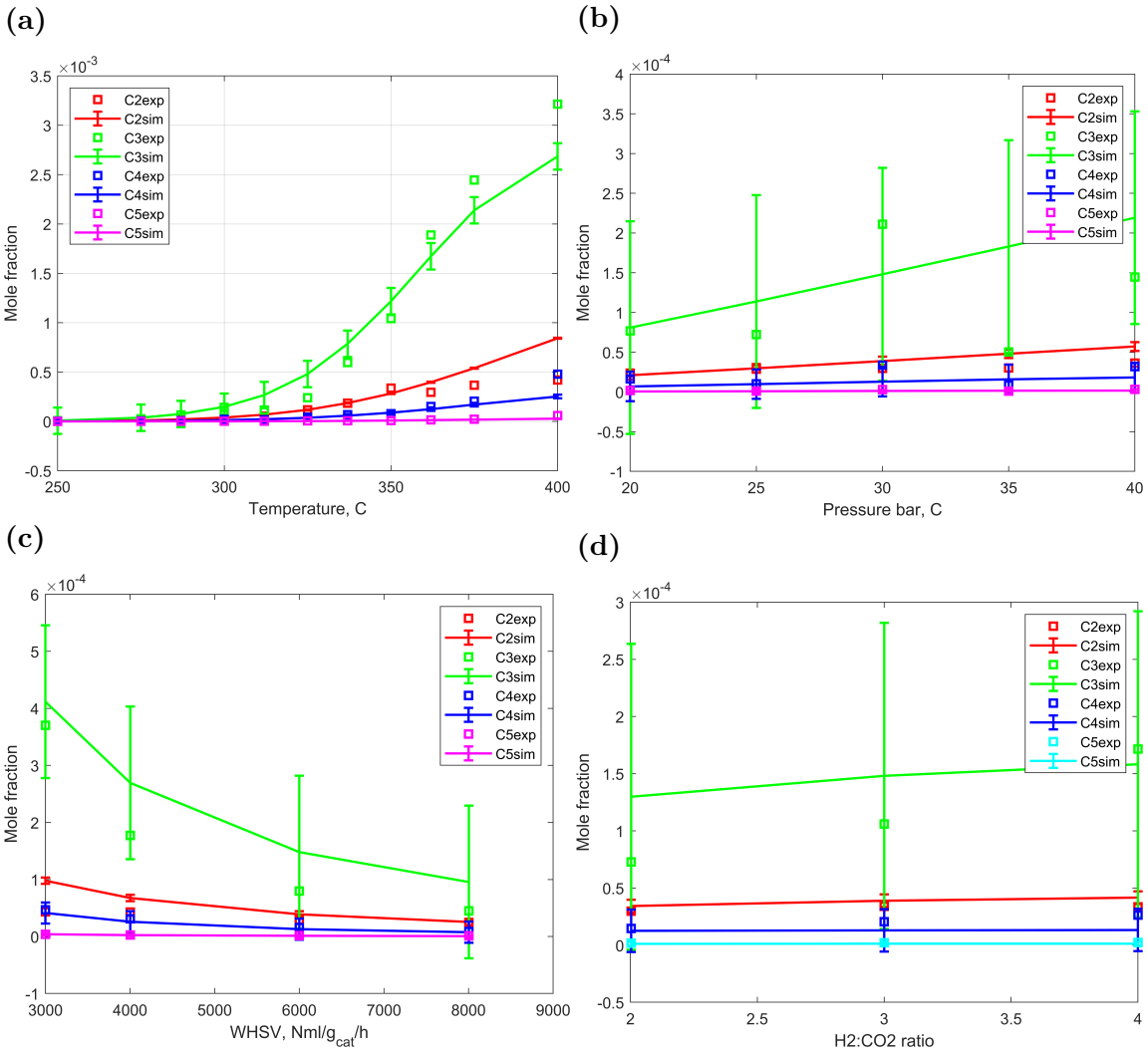


Figure 4.10: Model predictions of various paraffin molar fractions compared with the experimental results for varying temperature **(a)**, total pressure **(b)**, WHSV **(c)** and H_2:CO_2 molar feed ratio **(d)**. Unless otherwise indicated conditions are 300°C, 30 bar, 6000 Nml/g/h and 3:1 H_2:CO_2 molar feed ratio.

The ability of the model to predict the experimental data over different temperatures is shown in figure 4.10a. It is generally good but there are some difficulties to get an appropriate fit at high temperatures. The model is able to predict the drastic increase in propane concentration at high temperature but misses that the ethane concentration does not increase in the same way. The model is able to predict the other reactor conditions relatively well.

4.2.2.3 Methanol and methane predictions compared with experimental results

The model prediction of methanol and methane are compared with the experimental data in figure 4.11. The length of the bars are calculated in the same way as for figure 4.9.

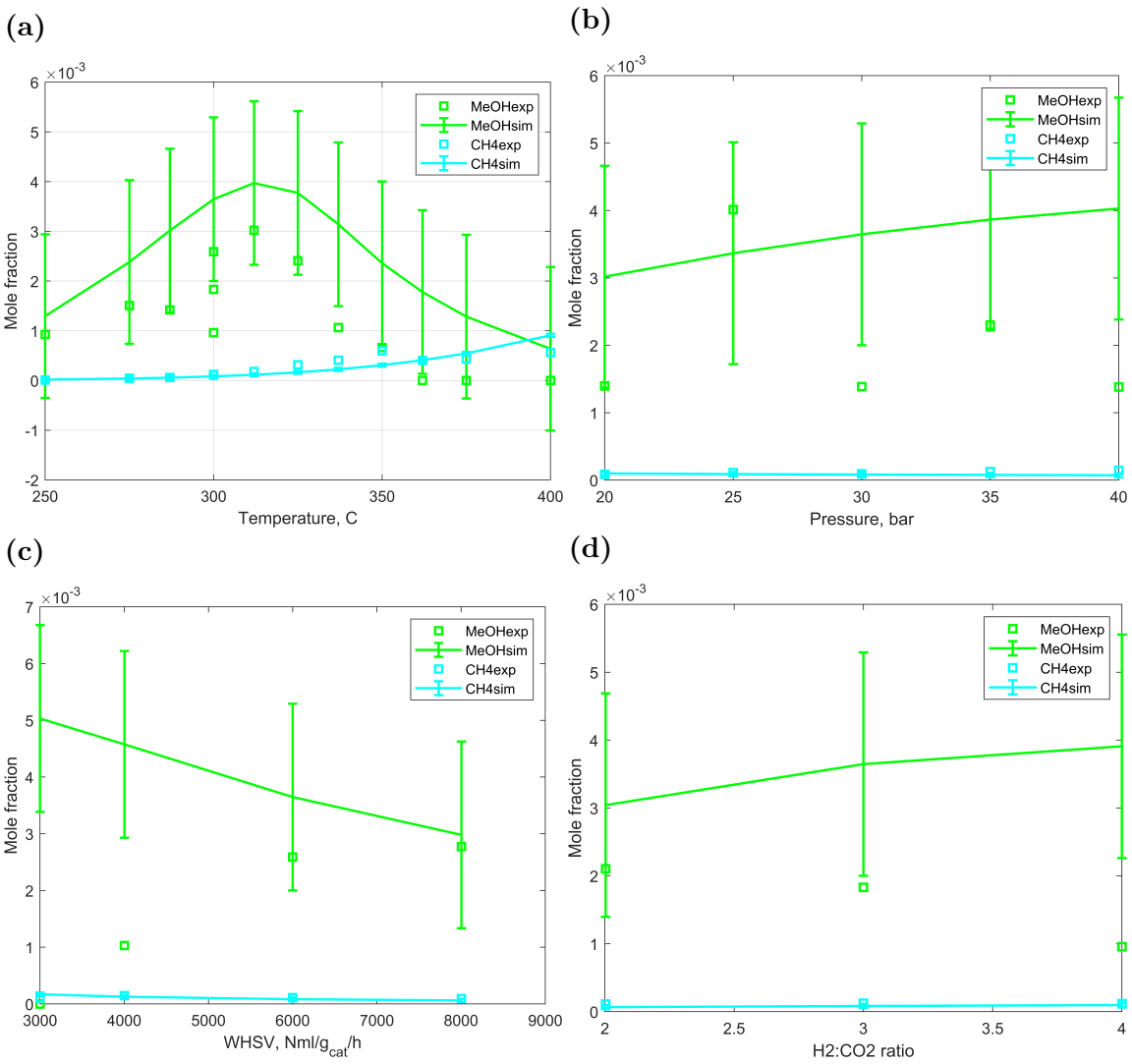


Figure 4.11: Model predictions of methanol and methane molar fractions compared with the experimental results for varying temperature **(a)**, total pressure **(b)**, WHSV **(c)** and H_2:CO_2 molar feed ratio **(d)**. Unless otherwise indicated conditions are 300°C, 30 bar, 6000 Nml/g/h and 3:1 H_2:CO_2 molar feed ratio.

Figure 4.11a shows that the model is able to predict the trend where the methanol molar fraction is at its highest around 312°C. There is a consistent overestimation of the methanol for most experiments and the variance of repeated experiments are quite high, which may be related to the deactivation of the zeolite. It may be solved by decreasing the rate constant for methanol production but there are not solid enough evidence as there are large variations in the data. The model predicts the trend opposite of the experiments in figure 4.11c and figure 4.11d. The error at different WHSV may be caused by the same reason that the olefins are underestimated at low WHSV, which is that the autocatalytic reactions rates should be higher than what they are in the model. The error concerning different H_2:CO_2 ratio is likely the same thing that was discussed in section 4.1.2.3, where the model does not have any part where H_2 partial pressure directly affects the consumption of methanol on the zeolite or that the autocatalytic reactions are underestimated.

The methane molar fractions are properly predicted by the model.

4.2.2.4 CO predictions compared with experimental results

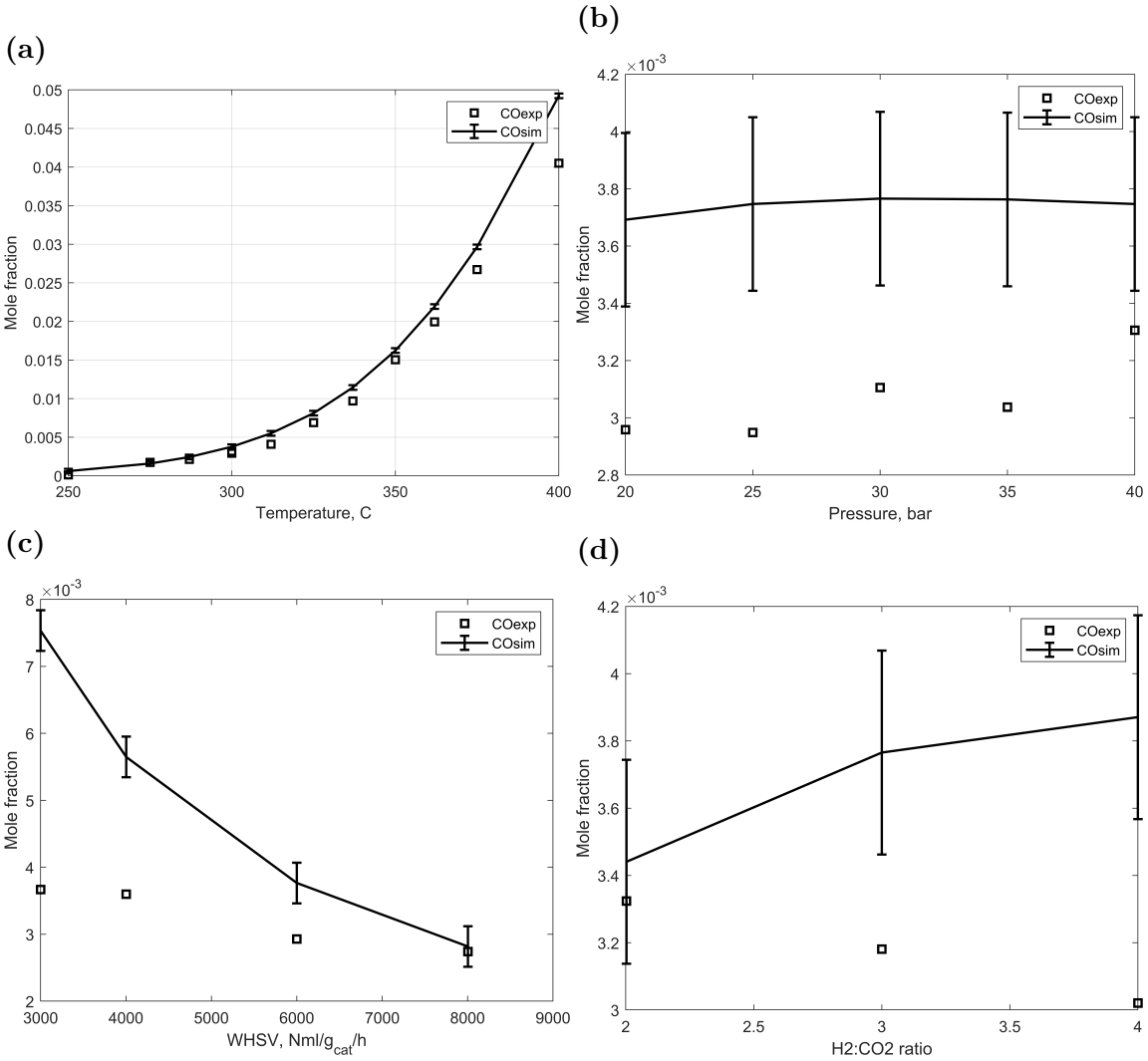


Figure 4.12: Model predictions of CO molar fraction compared with the experimental results for varying temperature **(a)**, total pressure **(b)**, WHSV **(c)** and H_2:CO_2 molar feed ratio **(d)**. Unless otherwise indicated conditions are 300°C, 30 bar, 6000 Nml/g/h and 3:1 H_2:CO_2 molar feed ratio.

In figure 4.12 the model predictions of CO molar fraction are compared with the experimental results. For different temperatures the model slightly overpredicts the molar fractions of CO. If figure 4.12a is compared with a similar figure that Ghosh *et al.* [13] had for their model and results it can be seen that the CO level is lower for the bifunctional catalyst at high temperatures. Ghosh *et al.* [13] has around 5.8 mol% of CO at 400 °C and around 0.5 mol% at 300 °C for otherwise similar conditions. This is consistent with what the reports that the RWGS reaction is suppressed in the bifunctional catalyst somewhat [25]. This is due to the fact that

the methanol synthesis is not thermodynamically limited in the bifunctional catalyst as the methanol produced is consumed by other reactions, which means that the methanol synthesis can compete against RWGS for consumption of CO_2. As the model overpredicts CO in general there may be some kinetic effects that suppresses the RWGS reaction more than just the thermodynamical effects that are known to be occurring in a bifunctional catalyst. It could also simply be an error from coming from the values of the parameters that Ghosh *et al.* had for the RWGS reaction on In_2O_3. Nevertheless, it is good that the model can predict the lower CO levels at high temperatures. In figure 4.12d the trends of the experiments and model prediction are the opposite of each other, but this may be nothing as the trend is very small. In figure 4.12c the model overpredicts the trend more at low WHSV then at high WHSV.

4.2.2.5 CO_2 predictions compared with experimental results

In figure 4.13 the model predictions of CO_2 molar fraction are compared with the experimental results and the molar fractions of H_2 from the model is also shown.

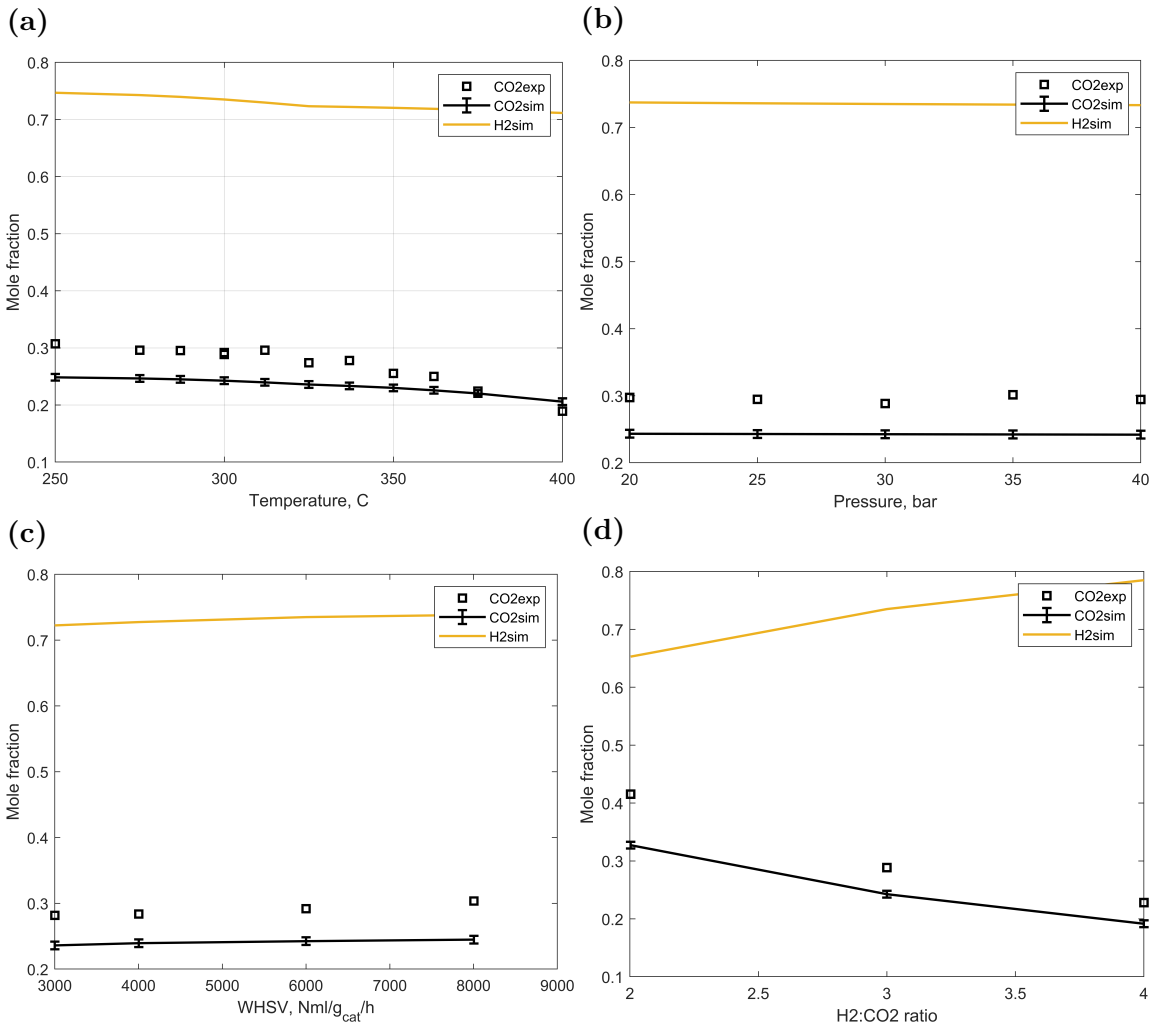


Figure 4.13: Model predictions of CO_2 molar fraction compared with the experimental results for varying temperature **(a)**, total pressure **(b)**, WHSV **(c)** and H_2:CO_2 molar feed ratio **(d)**. Unless otherwise indicated conditions are 300°C, 30 bar, 6000 Nml/g/h and 3:1 H_2:CO_2 molar feed ratio. The model prediction for H_2 is also shown.

In figure 4.13 the experimental molar fraction is larger than the model predicted molar fraction for all experiments except for two. Which are the same two experiments that has around 100 % carbon balance. With that in mind it is reasonable to assume that it is measurement errors on CO_2 that causes the carbon balance to be high. Which would also mean that the CO_2 conversion results in table 4.2 are not accurate. Otherwise the model predicts the trends for CO_2 well.

4.2.3 Model residual plots

In this section the residuals over different experiments are presented. As the residual plots provide little information that has not already been discovered by other means only the residuals of the olefins are presented here. The other residual plots can be found in appendix B.2. The residuals are the difference between the simulated molar fraction and the experimentally determined molar fraction and were calculated with equation 3.23 and the dotted lines in the plots are the range in which the residuals are within the range of the random errors of the repeated experiments (p value is 95%). Residual plots are helpful in finding systematic errors in the model and/or in the experiments as the residuals should be distributed randomly around 0 in the plot [35]. Figure 4.14 shows the residual plots of various olefins over temperature.

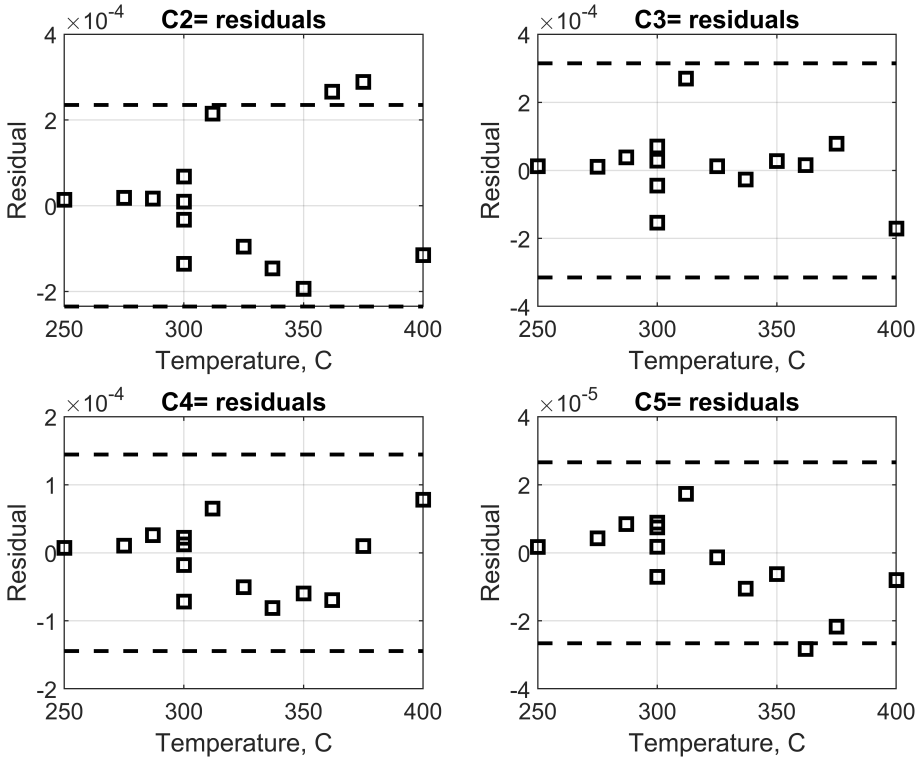


Figure 4.14: Residuals of olefins defined in equation 3.23 plotted along reactor temperature.

All residuals in figure 4.14 are normal in terms of magnitude but some have patterns at high temperatures. Ethylene seems to vary more around the prediction at higher temperatures than at lower temperatures. Likely cause of this is either that the model is not suited to predict ethylene at high temperature or that the variance of the experiments are higher at high temperature. Pentylene residuals are lowered at high temperatures, which means that the model underestimated the amount of pentylene at high temperatures. A possible fix for that is to adjust the activation energy for the pentylene producing reactions. In figure 4.15 the residual plots for the olefins over the chronological order of the experiments are shown.

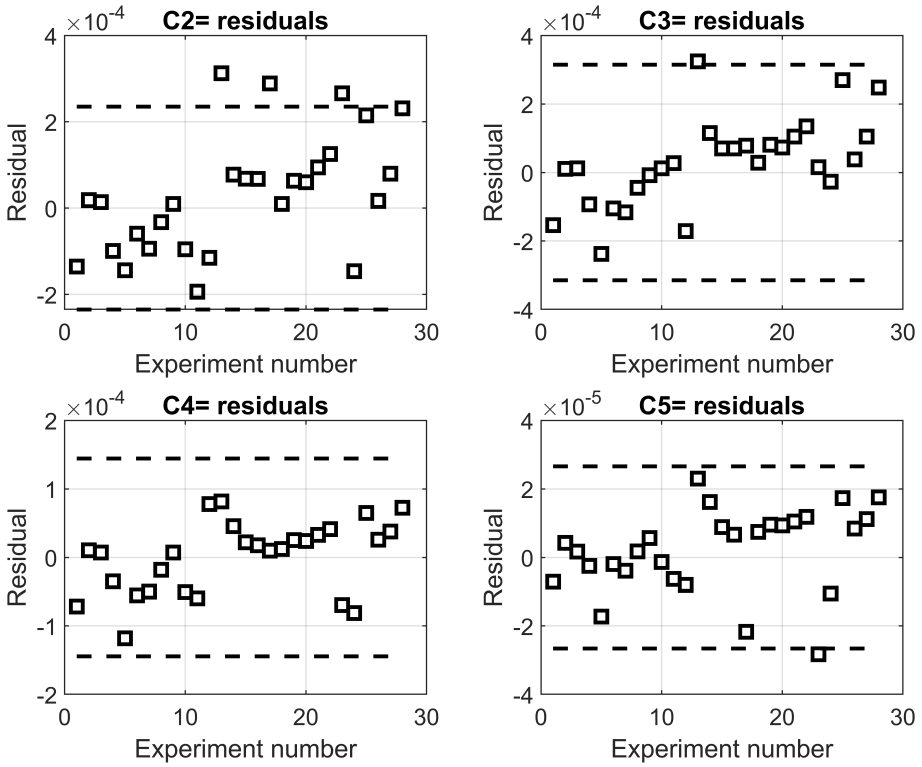


Figure 4.15: Residuals of olefins defined in equation 3.23 over the chronological order the experiment was conducted.

The magnitude of the residuals in figure 4.15 are all reasonable and there are no obvious signs that the variance of the experiments are increasing as the experimental procedure has progressed. However, a trend can be seen in all the residual plots in figure 4.15 where the residuals are increasing (in a non-absolute manner) as the experimental procedure progresses. This means that in the latter experiments the model is overpredicting the molar fraction outputs. The cause of this is most likely the slight deactivation of the zeolite which has been observed in section 4.1.2.4. For the residual plots of olefins over other parameters see appendix B.2.1.

4.2.4 Possibilities for improving the model

The model presented in section 4.2 has some flaws and it is important to discuss what may be done to improve it. The model should be compared with existing models with similar purposes. The In_2O_3 part of the model is taken from Ghosh *et al.* [13] and have not been changed and seem to correctly describe the behaviour for the In_2O_3. As for the zeolite part it was based on the work of Pérez-Uriarte *et al.* [18] that used a different zeolite with different framework structure. Therefore, many changes were necessary.

There are no models found in literature for this specific catalyst or any methanol mediated bifunctional catalyst that produces lower olefins from CO_2 directly. Therefore, there are no models to directly compare with. There are also no models for the MTO (methanol to olefins) for SSZ-13. However, Najafabadi *et al.* [36] have

developed a kinetic model on the MTO process for a similar catalyst, SAPO-34. The main difference between the model by Najafabadi *et al.* and the one in this thesis are:

- DME is included
- Propylene is formed from ethylene and DME yielding both propylene and methanol.
- Butylene and pentylene is formed in a similar way as propylene.
- Methanol can react to methane
- Only hydrogenation of ethylene was included

The scheme that Najafabadi *et al.* proposes is more consistent with the hydrocarbon pool scheme but it would be difficult to use for our data as there were no DME coming out from the reactor. The model by Najafabadi *et al.* at indicates that larger olefins forms from smaller olefins is reasonable.

As there are obvious signs of deactivation, there are reasons to try to model the coke formation on the zeolite to estimate the amount of deactivation. This would require a different kind of experimental plan as deactivation is time depended, whereas this model assumes that there is no deactivation and is independent of time. The other improvement that could be made easily from the data in this work is to not lump the olefin hydrogenation. If that is done the hydrogenation reactions can have independent activation energies which will give a better fit.

4.3 Further work in this topic

There are many more things that can be further researched and improved with different kinds of experiments. As there are signs of deactivation it may be appropriate to redo the experiments in this work using a higher temperature for the standard reaction conditions. That way it is possible to reduce the amount of deactivation in the reactions and get better experimental results. It may also be of interest to optimise the reaction conditions in some way to find the optimal reaction conditions to use as the standard conditions for future experiments. Currently the model is centred around 300 °C, which is a bit low for the zeolite. I would suggest to rise that to 325 °C. Another possible improvement is to before conducting experiments at various conditions is to run the reaction for some hours to get it into steady state (if possible) with purpose to of getting an steady hydrocarbon pool. This could possibly make the experiments more consistent and if conditions would be returned to standard conditions between every set of conditions to better track variations and catalyst deactivation.

Other experimental work that can be done in order to both validate and improve the model is to perform experiments with different mass ratio of In_2O_3:SSZ-13 and see how well the model is able to predict different mass ratios. Another thing that can be done is to feed other species than H_2 and CO_2 into reactor such as methanol, DME, CO, H_2O and lower olefins. If that is done it is easier to resolve some of

the kinetic parameters (their normalised sensitivity coefficients will be higher). It is especially of interest to feed DME as no DME was found in the reactor outlet during experiments even though it was expected to be found. If the DME is fed into the reactor or the reactor is operated where DME is expected to be present in the reactor effluent, it is possible to also evaluate to DME to olefins reactions. A higher In_2O_3/SSZ-13 ratio would likely increase amount of methanol and DME in the reactor effluent.

Future work can be done in looking how mass transfer affects the selectivity of the different compounds using the same method as the work presented in appendix C but with this model for producing lower olefins. Other work that can be done is that the optimisation of the In_2O_3 and SSZ-13 catalyst to be more active, selective and resistant to deactivation.

5
Conclusion

In this work, a kinetic model for the methanol mediated hydrogenation of CO_2 to lower olefins has been developed for a bifunctional catalyst containing In_2O_3 and the zeolite SSZ-13. It has not been possible to accurately predict the CO_2 conversion due to issues with measurement of CO_2 in the reactor effluent. From the experiments it can be concluded that the reaction is consistent with what has been reported earlier and that there is deactivation of the zeolite at low temperatures. The deactivation means that the reactor should be operated at a temperature higher than 300 °C.

The model developed has the ability to predict the experimental data for the most part with some improvement that may be made by adjusting the kinetic parameters for the autocatalytic reactions and perhaps adding or changing some reactions. Nevertheless, this model can be considered a starting point for future models and the kinetic model works reasonably well for predicting the lower olefins, which are the main products. Further validation of this model is needed and it is likely that the catalyst needs development and therefore the kinetic parameters will be changed.

Bibliography

[1] Ma Z, Porosoff MD. Development of Tandem Catalysts for CO_2 Hydrogenation to Olefins. ACS Catalysis. 2019;9(3):2639–2656. Available from: `https://doi.org/10.1021/acscatal.8b05060`.

[2] Sharma P, Sebastian J, Ghosh S, Creaser D, Olsson L. Recent advances in hydrogenation of CO_2 into hydrocarbon via methanol intermediate over heterogeneous catalysts. Catalysis Science & Technology. 2021.

[3] Goud D, Gupta R, Maligal-Ganesh R, Peter SC. Review of Catalyst Design and Mechanistic Studies for the Production of Olefins from Anthropogenic CO_2. ACS Catalysis. 2020;10:14258–14282.

[4] Ronda-Lloret M, Rothenberg G, Shiju NR. A critical look at direct catalytic hydrogenation of Carbon dioxide to olefins. ChemSusChem. 2019;12:3896–3914.

[5] Dang S, Gao P, Liu Z, Chen X, Yang C, Wang H, et al. Role of zirconium in direct CO_2 hydrogenation to lower olefins on oxide/zeolite bifunctional catalysts. Journal of Catalysis. 2018;364:382–393.

[6] Numpilai T, Wattanakit C, Chareonpanich M, Limtrakul J, Witoon T. Optimization of synthesis condition for CO_2 hydrogenation to light olefins over In_2O_3 admixed with SAPO-34. Energy Conversion and Management. 2019;180:511–523.

[7] Renken A, Kiwi-Minsker L. Catalytic Reaction Engineering Principles. In: Beller M, Renken A, van Santen RA, editors. Catalysis. Weinheim: Wiley-VCH Verlag & Co; 2013. p. 67–112.

[8] Martin O, Martín AJ, Mondelli C, Mitchell S, Segawa TF, Hauert R, et al. Indium Oxide as a Superior Catalyst for Methanol Synthesis by CO_2 hydrogenation. Angewandte Chemie International Edition. 2016;55(21):6261–6265.

[9] Huš M, Dsireddy VDBC, Štefančič NS, Likozar B. Mechanism, kinetics and thermodynamics of carbon dioxide hydrogenation to methanol on $Cu/ZnAl_2O_4$ spinel-type heterogeneous catalysts. Applied catalysis B: Enviromental. 2017;27:267–278.

[10] Martin NM, Velin P, Skoglundh M, Bauer M, Carlsson PA. Catalytic hydrogenation of CO_2 to methane over supported Pd, Rh and Ni catalysts. Catalysis Science & Technology. 2017;7:1086–1094.

[11] Ye J, Liu C, Ge Q. DFT Study of CO_2 Adsorption and Hydrogenation on the In_2O_3 Surface. Journal of Physical Chemistry. 2012;116:7817–7825.

[12] Ye J, Liu C, Mei D, Ge Q. Active Oxygen Vacancy Site for Methanol Synthesis from CO_2 Hydrogenation on $In_2O_3(110)$: A DFT Study. ACS Catalysis. 2013;6:1296–1306.

[13] Ghosh S, Sebastian J, Olsson L, Creaser D. Experimental and kinetic modeling studies of methanol synthesis from CO_2 hydrogenation using In_2O_3 catalyst. Chemical Engineering Journal. 2021;416:129120.

[14] Bhatia S. 1. In: Zeolite Catalysis: Principles and Applications. Boca Raton, Florida: CRC Press; 1990. p. 1–6.

[15] Wu L, Hensen EJM. Comparison of mesoporous SSZ-13 and SAPO-34 zeolite catalysts for the methanol-to-olefins reaction. Catalysis Today. 2014;235:160–168.

[16] Bleken F, Bjørgen M, Palumbo L, Bordiga S, Svelle S, Lillerud KP, et al. The effect of acid strength on the conversion of methanol to olefins over acidic microporous catalysts with the CHA topology. Topics in Catalysis. 2009;52:218–228.

[17] Wang A, Chen Y, Walter ED, Washton NM, Varha T, Wang Y, et al. Remarkable self-degredation of Cu/SAPO-34 selective catalytic reduction catalysts during storage at ambient conditions. Catalysis today. 2021;360:367–374.

[18] Pérez-Uriarte P, Ateka A, Aguayo AT, Gayubo AG, Bilbao J. Kinetic model for the reacto of DME to olefins over a HZSM-5 zeolite catalyst. Chemical Engineering Journal. 2016;302:801–810.

[19] Chowdhury AD, Houben K, Whithing GT, Makhtar M, Asiri AM, Al-Thabaiti SA, et al. Initial Carbon–Carbon Bond Formation during the Early Stages of the Methanol-to-Olefin Process Proven by Zeolite-Trapped Acetate and Methyl Acetate. Angewandte Chemie International Edition. 2016;55(51):15840–15845.

[20] Li J, Wei Z, Chen Y, Jinh B, He Y, Dong M, et al. A route to form initial hydrocarbon pool species in methanol conversion to olefins over zeolites. Journal of Catalysis. 2014;317:277–283.

[21] Dessau RM, LaPierre RB. On the mechanism of methanol conversion to hydrocarbons over HZSM-5. Journal of Catalysis. 1982;78(1):136–141.

[22] Dahl IM, Kolboe S. On the Reaction Mechanism for Hydrocarbon Formation from Methanol over SAPO-34: I. Isotopic Labeling Studies of the Co-Reaction of Ethene and Methanol. Journal of Catalysis. 1994;149(2):458–464.

[23] Hwang A, Bhan A. Deactivation of Zeolites and Zeotypes in Methanol-to-HydrocarbonsCatalysis: Mechanisms and Circumvention. Accounts of chemical research. 2019;52:2647–2656.

[24] Gao P, Dang S, Li S, Bu X, Liu Z, Qiu M, et al. Direct Production of Lower Olefins from CO_2 Conversion via Bifunctional Catalysis. ACS Catalysis. 2018;8:571–578.

[25] Gao P, Li S, Bu X, Dang S, Liu Z, Wang H, et al. Direct conversion of CO_2 into liquid fuels with high selectivity over a bifunction catalyst. Nature Chemistry. 2017;9:1019–1024.

[26] Wang J, Zhang A, Jiang X, Song C, Guo X. Highly selective conversion of CO_2 to lower hydrocarbons C_2-C_4) over bifunctional catalysts composed in In_2O_3-ZrO_2 and zeolite. Journal of CO_2 utilization. 2018;27:81–88.

[27] Wei J, Ge Q, Yao R, Wen Z, Fang C, Guo L, et al. Directly converting CO_2 into a gasoline fuel. Nature Communications. 2017;8:1–8.

[28] Cheng K, Zhou W, Kang J, He S, Shi S, Zhang Q, et al. Bifunctional catalysts for one-step conversion of syngas into aromatics with excellent selectivity and stability. Chemistry. 2017;3:334–347.

[29] Frei MS, Modelli C, García-Muelas R, Kley KS, Puértolas B, López N, et al. Atomic-scale engineering of indium oxide promotion by palladium for methanol production via CO_2 hydrogenation. Nature Communications. 2019;10:1–11.

[30] Li Z, Navarro MT, Marínez-Triguero J, Yu J, Corma A. Synthesis of nano-SSZ-13 and its application in the reaction of methanol to olefins. Catalysis Science & Technology. 2016;6:5856–5863.

[31] Schlögl R. X-ray Diffraction: A Basic Tool for Characterization of Solid Catalysts in the Working State. In: Gates BC, Knözinger H, editors. Advances in Catalysis. London: Academic Press; 2009. p. 273–338.

[32] Towler G, Sinnott R. 15. In: Chemical Engineering Design. 2nd ed. The Boulevard, Langford Lane, Kidlington, Oxford, OX5 1GB, UK: Elsevier Science & Technology; 2012. p. 631–752.

[33] Mears DE. Tests for Transport Limitations in Experimental Catalytic Reactors. Industrial & Engineering Chemistry Process Design and Development. 1971;10:541–547.

[34] Weisz PB, Prater CD. Interpretation of measurements in experimental catalysis. Advances in Catalysis. 1954;6:143–196.

[35] Rasmuson A, Andersson B, Olsson L, Andersson R. Mathematical Modeling in Chemical Engineering. Cambridge CB2 8BS, United Kingdom: Cambridge University Press; 2014.

[36] Najafabadi AT, Fatemi S, Sohrabi M, Salmasi M. Kinetic modeling and optimazation of the operating condition of MTO process on SAPO-34 catalyst. Journal of Industrial and Engineering Chemistry. 2012;18:29–37.

[37] Poling BE, Prausnitz JM, O'Connell JP. Properties of Gases and Liquids. London: McGraw-Hill Education; 2001.

[38] Scott H, Fogler. Elements of chemical reaction engineering. 5th ed. Boston: Prentice Hall; 2016.

A

Appendix - Reactor model assumptions

In the reactor model, assumptions regarding isobaric conditions and negligible inner- and outer mass transfer limitations was done. In this appendix, the calculations for confirming these assumption are presented.

A.1 Estimation of physical properties

As the calculations below requires physical properties such as viscosity, diffusivity and density estimation of them must be made. All estimations assumes the composition of the inlet.

A.1.1 Fluid density

Estimation of the fluid density is done by assuming ideal gas which gives the following equation.

$$\rho = \frac{MP}{RT} \tag{A.1}$$

Where ρ is the fluid density, M is the molecular weight of the mixture, P is the pressure, R is the gas constant and T is the temperature. The mixture density is assumed to be

$$\rho_f = \sum_i y_i \rho_i \tag{A.2}$$

Where y_i is the molar fraction of specie i.

A.1.2 Fluid viscosity

The fluid viscosity is estimated by equation A.3 [37].

$$\mu = \frac{16.64(M)^{1/2}T}{(\varepsilon/k)^{1/2}\sigma^2} \tag{A.3}$$

Where μ is the dynamic viscosity of the fluid, ε is the minimum of pair-potential energy, k is the Boltzmann constant and σ is the hard-sphere diameter of the molecule. The mixture viscosity is assumed to be

$$\mu = \sum_i y_i \mu_i. \tag{A.4}$$

A.1.3 Diffusivity

The diffusivity calculations calculates a binary diffusivity between component A which is a mixture of CO_2 and H_2 and a component B which is an arbitrarily chosen species *i*. The diffusivity is estimated with Chapman-Enskog theory assuming ideal gas and is calculated as [37]

$$D_{\mathrm{AB}} = \frac{0.00266 T^{3/2}}{P M_{\mathrm{AB}}^{1/2} \sigma_{\mathrm{AB}}^2 \Omega_D}. \tag{A.5}$$

Where $M_{AB} = 2(1/M_{Mixture} + 1/M_i)^{-1}$, $\sigma_{AB} = (\sigma_{Mixture} + \sigma_i)/2$ and Ω_D is a dimensionless collision integral and calculated as [37]

$$\Omega_D = \frac{A}{(T^*)^{\mathrm{B}}} + \frac{C}{\exp(DT^*)} + \frac{E}{\exp(FT^*)} + \frac{G}{\exp(HT^*)} \tag{A.6}$$

Where $A = 1.06036$, $B = 0.1561$, $C = 0.19300$, $D = 0.47635$, $E = 1.03587$, $F = 1.52996$, $G = 1.76474$, $H = 3.89411$ and $T^* = kT/\varepsilon_{AB}$. ε_{AB} is calculated by [37]

$$\varepsilon_{AB} = (\varepsilon_{Mixture} \cdot \varepsilon_i)^{1/2}. \tag{A.7}$$

A.2 Pressure drop calculation

The isobaric conditions can be confirmed by estimating the pressure drop in the reactor. This can be done with the Ergun equation [32].

$$\frac{\Delta P}{L_b} = 150 \frac{(1-\varepsilon)^2}{\varepsilon^3} \frac{\mu u}{d_p^2} + 1.75 \frac{(1-\varepsilon)}{\varepsilon^3} \frac{\rho_f u^2}{d_p} \tag{A.8}$$

Where ΔP is the pressure drop, L_b is the length of the reactor bed, $\varepsilon = 0.3$ is the bed porosity, μ is the dynamic viscosity of the gas calculated by equation A.3, u is the superficial fluid velocity and $d_p = 375$ μm is the particle diameter.

The maximum pressure drop in the reactor estimated in all of the experiments were 28 Pa when the reactor conditions were 20 bars, 300 °C, 6000 Nml g_{cat}^{-1} h^{-1} and 3:1 H_2:CO_2 molar ratio. Since the estimated pressure drop is so low it is reasonable to assume that the reactor were operated isobarically.

A.3 Mears parameter calculation

The Mears parameter is a dimensionless number where the observed reaction rate is compared to the maximum mass transport from the bulk fluid to the surface of the catalyst [33].

$$\text{MP} = \frac{\rho_f r_{obs} d_p}{2 k_c C_b} \tag{A.9}$$

Where ρ_f is the fluid density, r_{obs} is the observed reaction rate in mol kg^{-1} s^{-1}, $d_p = 375$ μm is the diameter of the catalyst particle, C_b the concentration in the bulk fluid and k_c is the outer mass transfer coefficient. In a packed bed of spherical particles, the Thoenes-Kramers correlation can be used [38].

$$\frac{k_c d_p}{D_{AB}} \cdot \frac{\varepsilon}{1-\varepsilon} \cdot \frac{1}{\gamma} = \left(\frac{u d_p \rho_f}{\mu (1-\varepsilon) \gamma} \right)^{1/2} \left(\frac{\mu}{\rho_f D_{AB}} \right)^{1/3} \tag{A.10}$$

Where D_{AB} is diffusivity, ε is the void fraction of the packed bed, γ is a shape factor (equal to one for spheres) and u is the superficial velocity.

For all the experiments and all the species the largest value of the Mears parameter was 0.0012 for pentane for the experiments at 30 bars, 250 °C, 6000 Nml g_{cat}^{-1} h^{-1} and 3:1 H_2:CO_2 molar ratio. This means that during the experiment the reactions were never limited by the diffusion inside the catalyst particles.

A.4 Weisz-Prater parameter calculation

The Weisz-Prater parameter is a dimensionless number where the observed reaction rate is compared to the maximum mass transport through the catalyst andis calculated as [34]

$$\text{WP} = \frac{r_{obs} \rho_C d_p^2}{4 D_{eff} C_s} \tag{A.11}$$

Where $\rho_C = 2000 kgm^{-3}$, D_{eff} is the effective diffusivity and C_s is the concentration in the catalyst surface. The effective diffusivity is assumed to be a tenth of the molecular diffusivity and the surface concentration the same as the bulk concentration.

For all the experiments and all the species the largest value of the Weisz-Prater parameter was 0.37 for pentane for the experiments at 30 bars, 250 °C, 6000 Nml g_{cat}^{-1} h^{-1} and 3:1 H_2:CO_2 molar ratio. This means that the outer mass transfer should not be completely disregarded but that it may have affected the observed reaction rate somewhat. By this effect is small and limited to the experiments at low temperature (low diffusion of the larger hydrocarbons) and should not have affected the experiments significantly at other conditions.

B

Appendix - Results

As there were many results to report in this thesis to report. Some did not make it to the main report. Those results that are not presented in the report are presented here.

B.1 Experimental results

B.1.0.1 The influence of total pressure on catalytic activity

CO_2 conversion and carbon selectivities over different reactor pressures are shown in figure B.1.

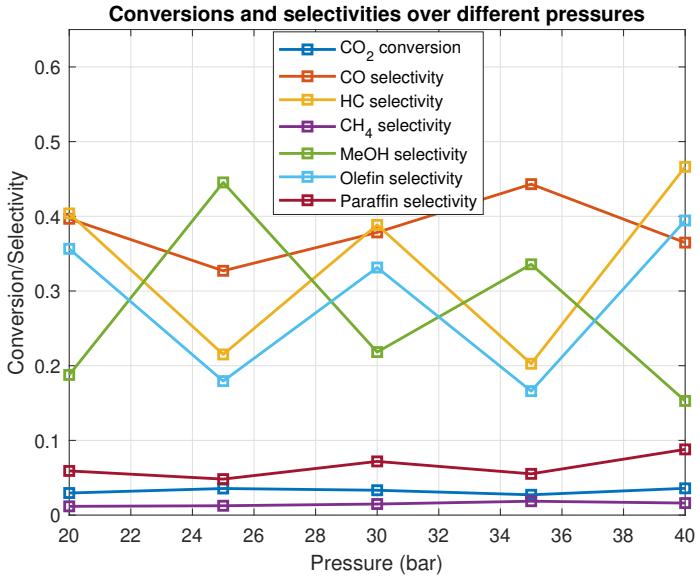


Figure B.1: Carbon selectivities and CO_2 conversion calculated with equation 3.3 and equation 3.2 respectively over different reactor pressures. Experiments included are 2a, 2b, 2c, 5e and 5f.

As experiments 5e and 5f seemingly breaks the trend it is difficult to reach any conclusion without ignoring experiment 5e and 5f. Since they were carried out at several weeks later the catalyst may have been affected. If experiments 5e and 5f are ignored there are only weak trends to observe. CO_2 conversion as well as olefin selectivity is the highest at 30 bars and lowest at 20 bars. It seems from this data

that 30 bars is a reasonable operating pressure for the reactor.

In figure B.2 the distribution of different hydrocarbons over different total reactor pressures is shown.

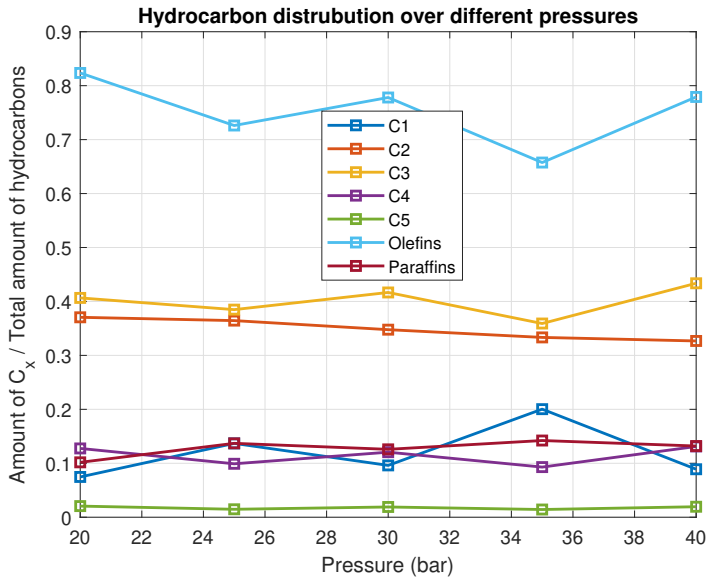


Figure B.2: Molar based hydrocarbon distribution over different pressures. Note that CH_4 is not included among paraffins. Experiments included are 2a, 2b, 2c, 5e and 5f.

In a similar fashion to figure B.1, figure B.2 does not contain any clear trends. Therefore the pressure does not effect the hydrocarbon distribution in any significant matter.

B.2 Model residual plots

B.2.1 Olefin residual plots

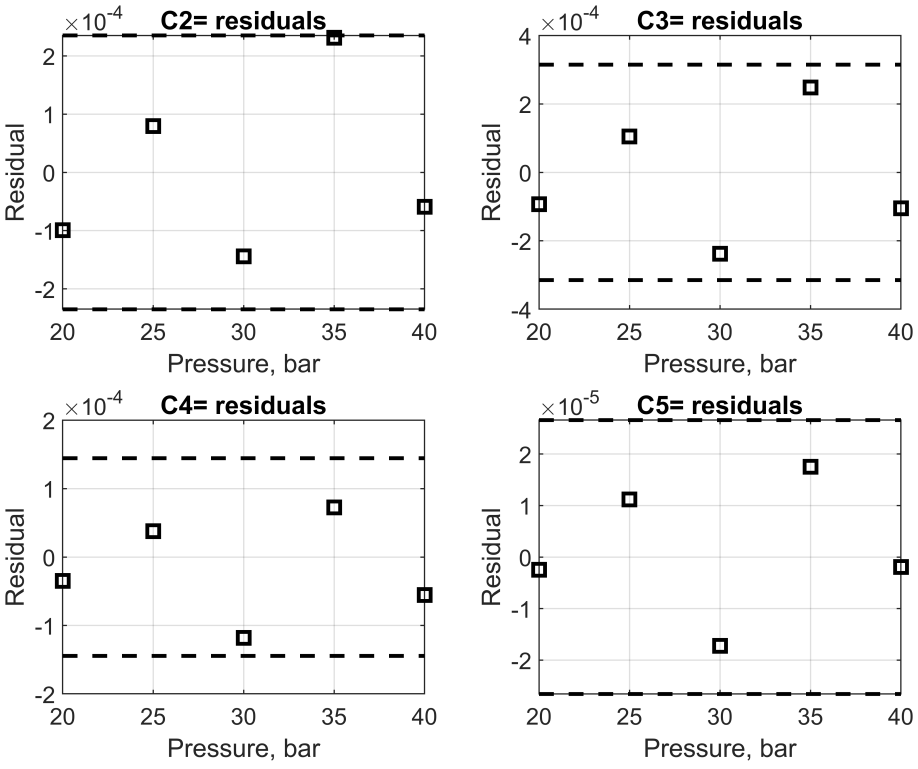


Figure B.3: Residuals of olefins defined in equation 3.23 plotted along reactor pressure.

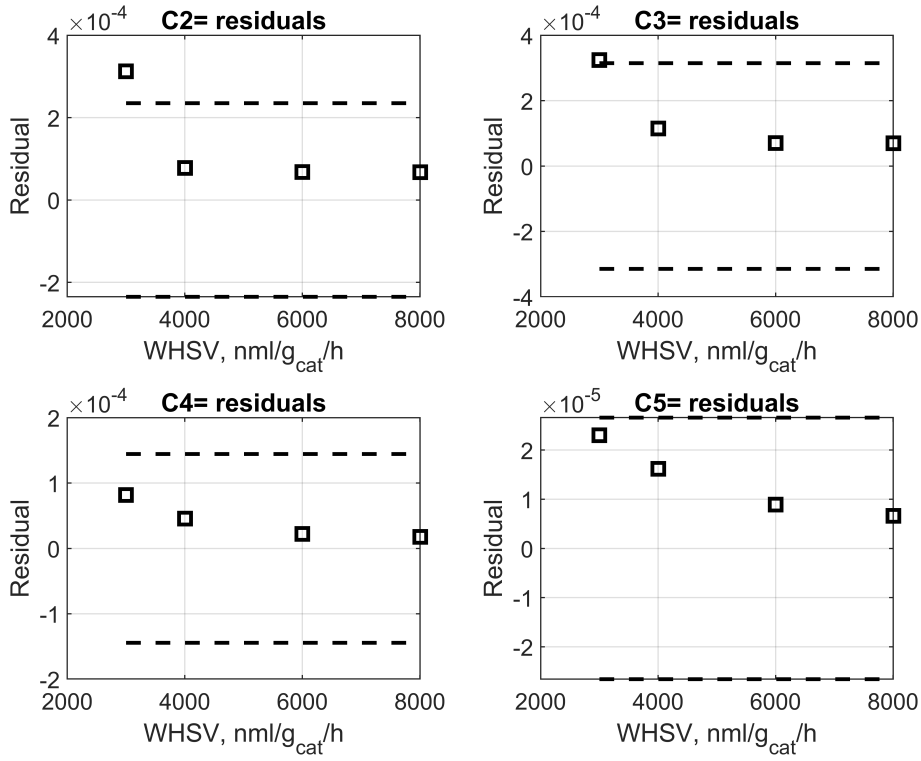


Figure B.4: Residuals of olefins defined in equation 3.23 plotted along WHSV.

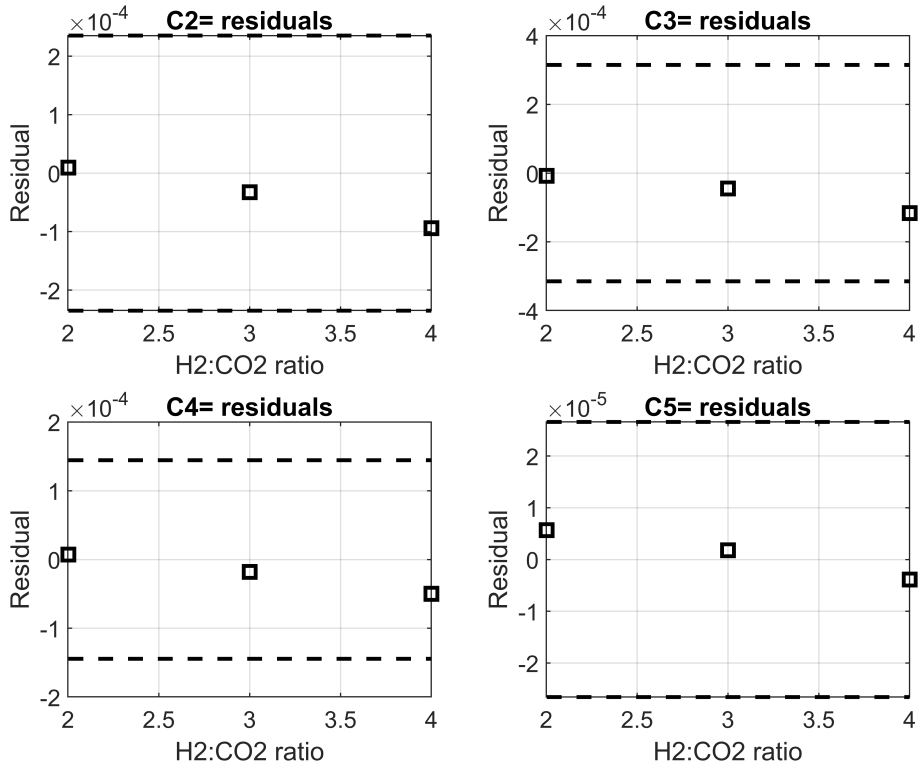


Figure B.5: Residuals of olefins defined in equation 3.23 plotted along H_2:CO_2 ratio.

B.2.2 Paraffin residual plots

Figure B.6 shows the residual plots of various paraffins over temperature.

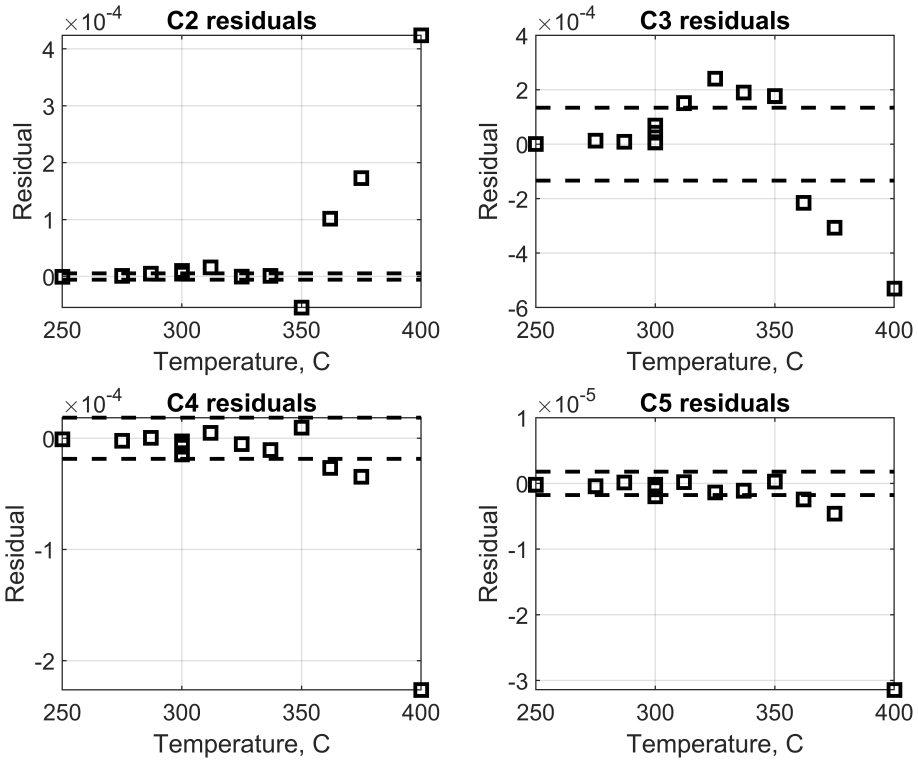


Figure B.6: Residuals of paraffins defined in equation 3.23 plotted along reactor temperature.

The residuals in figure B.6 shows that that the model prediction start to become worse at high temperature but are decent below 350 °C.

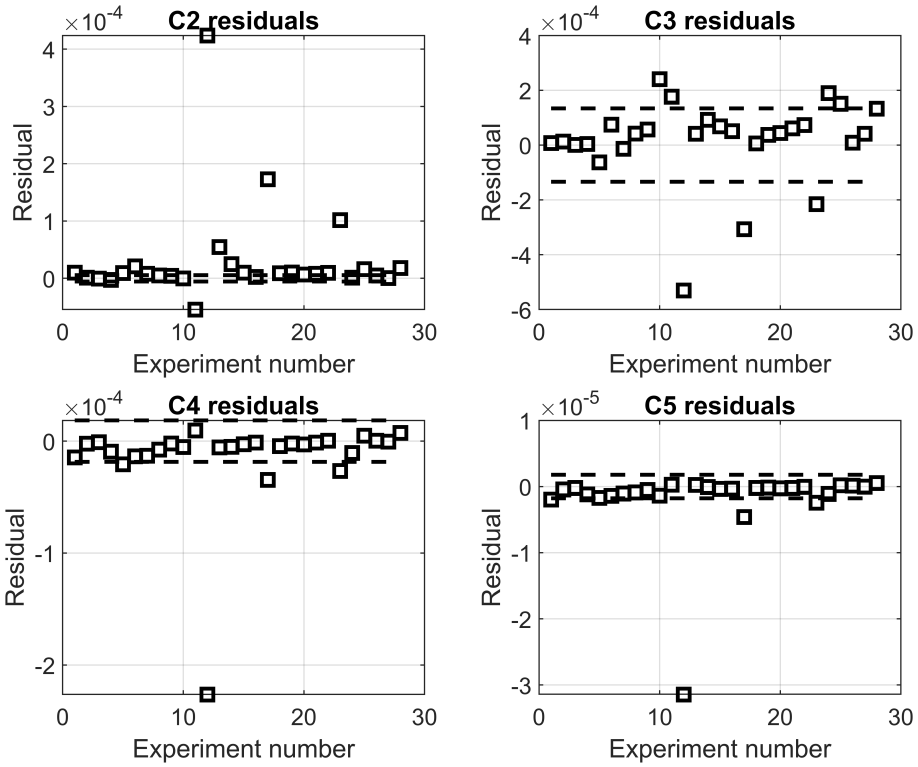


Figure B.7: Residuals of paraffins defined in equation 3.23 over the chronological order the experiments were conducted.

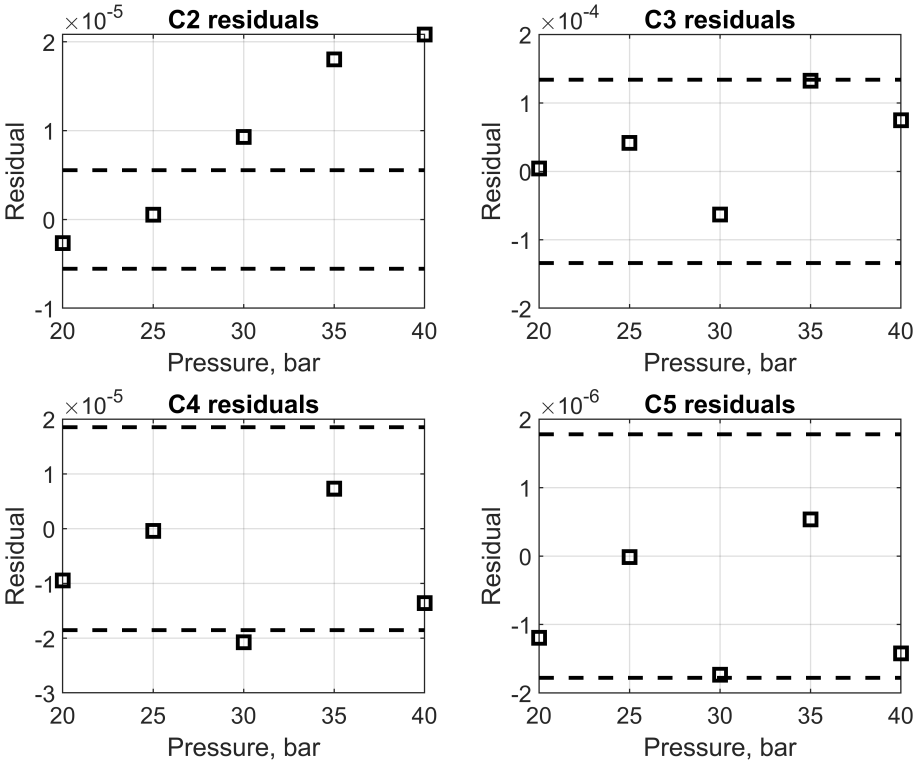


Figure B.8: Residuals of paraffins defined in equation 3.23 plotted along reactor pressure.

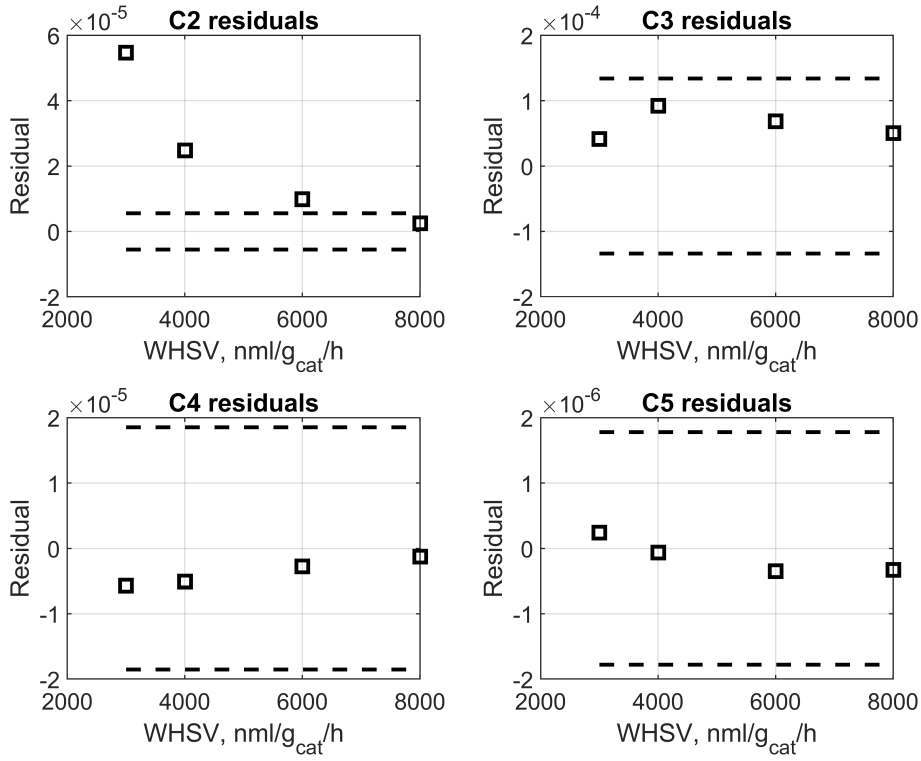


Figure B.9: Residuals of paraffins defined in equation 3.23 plotted along WHSV.

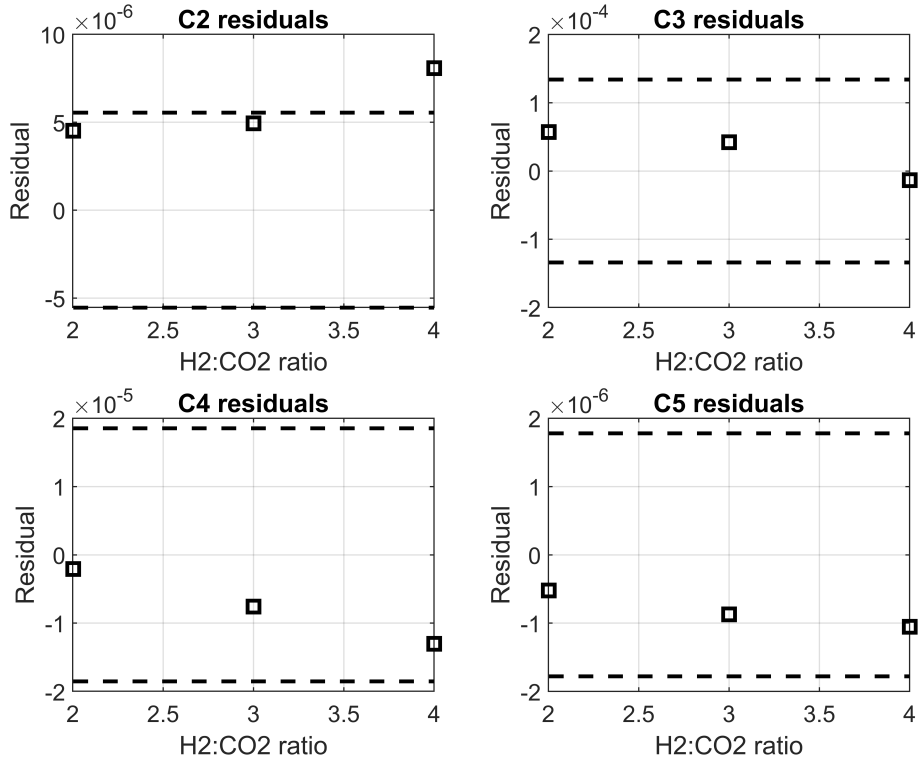
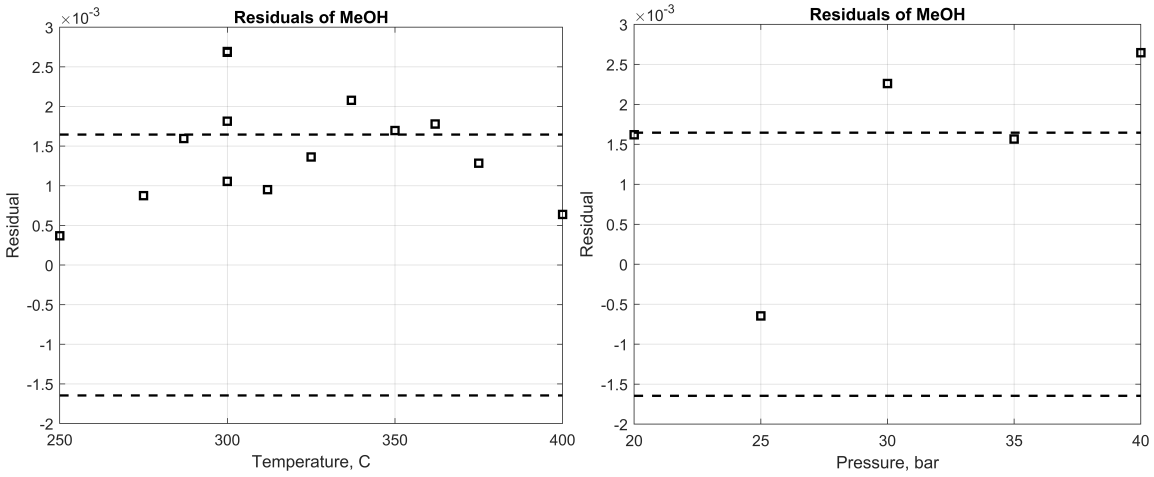


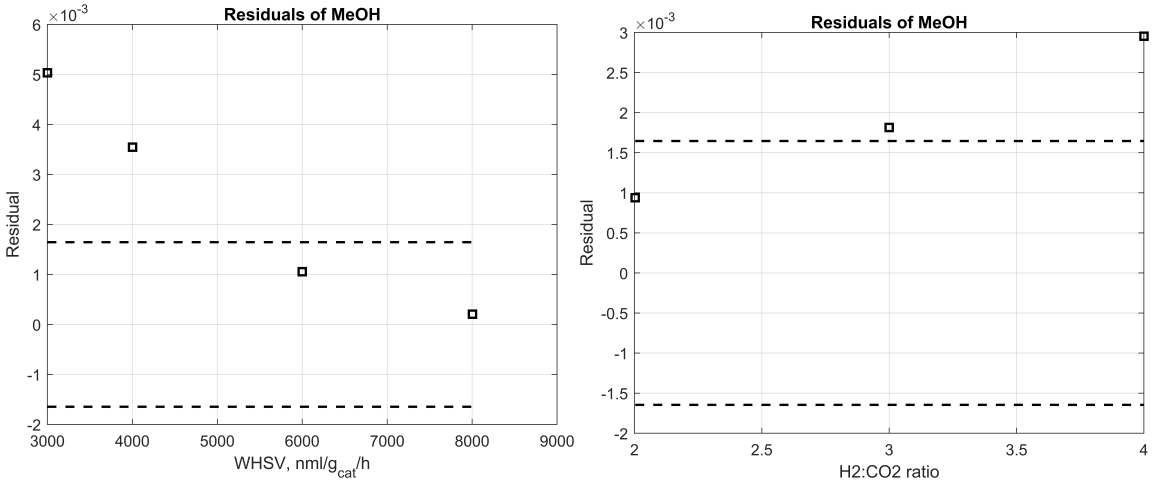
Figure B.10: Residuals of paraffins defined in equation 3.23 plotted along H_2:CO_2 ratio.

B.2.3 Methanol residual plots



(a) W.r.t temperature.

(b) W.r.t pressure.



(c) W.r.t WHSV

(d) W.r.t H_2:CO_2 ratio

Figure B.11: Residual plots of methanol defined in equation 3.23 over different reactor conditions

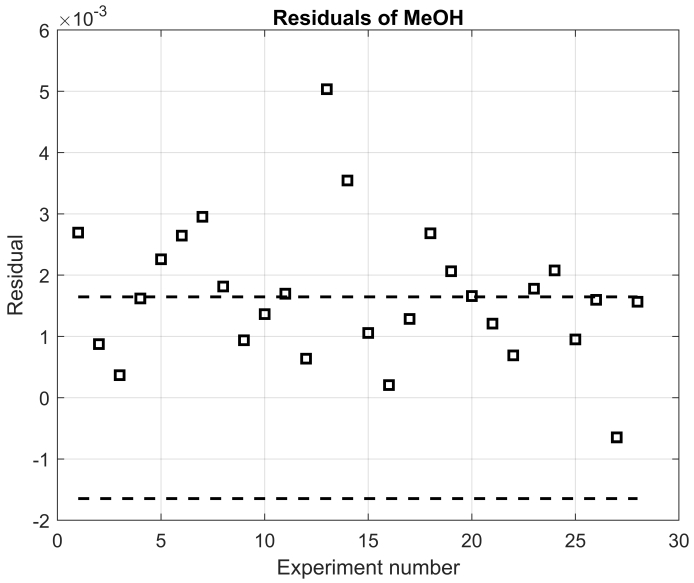
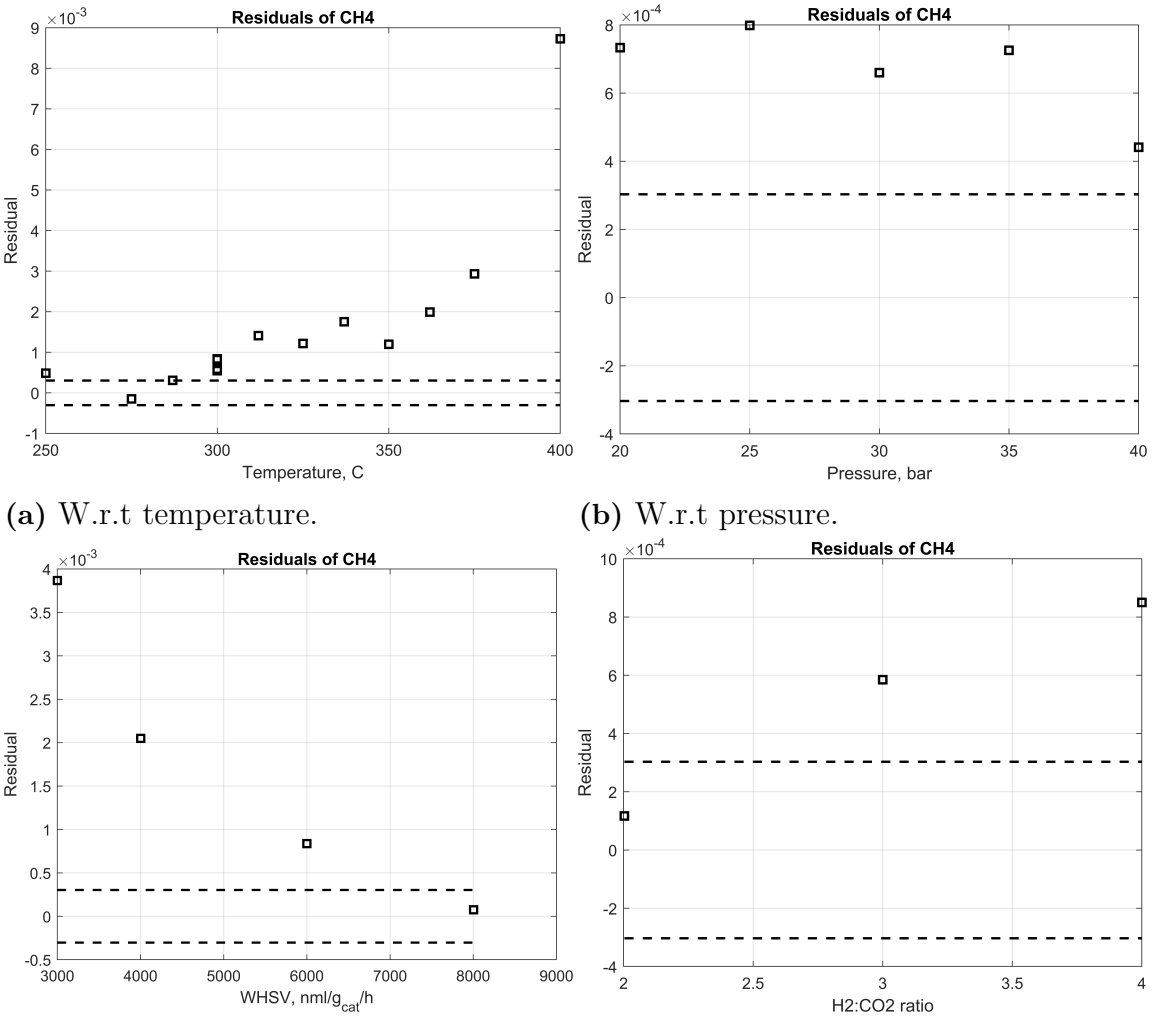


Figure B.12: Residuals of methanol defined in equation 3.23 over the chronological order of the experiments were conducted.

B.2.4 Methane residual plots



(a) W.r.t temperature.

(b) W.r.t pressure.

(c) W.r.t WHSV

(d) W.r.t H_2:CO_2 ratio

Figure B.13: Residual plots defined in equation 3.23 of methane over different reactor conditions

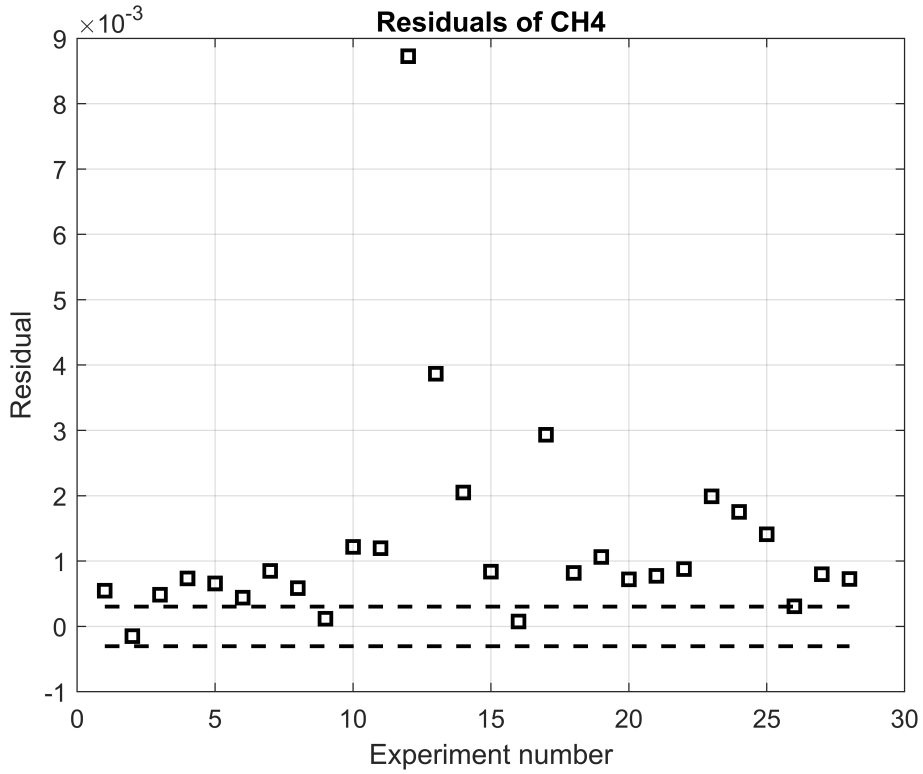
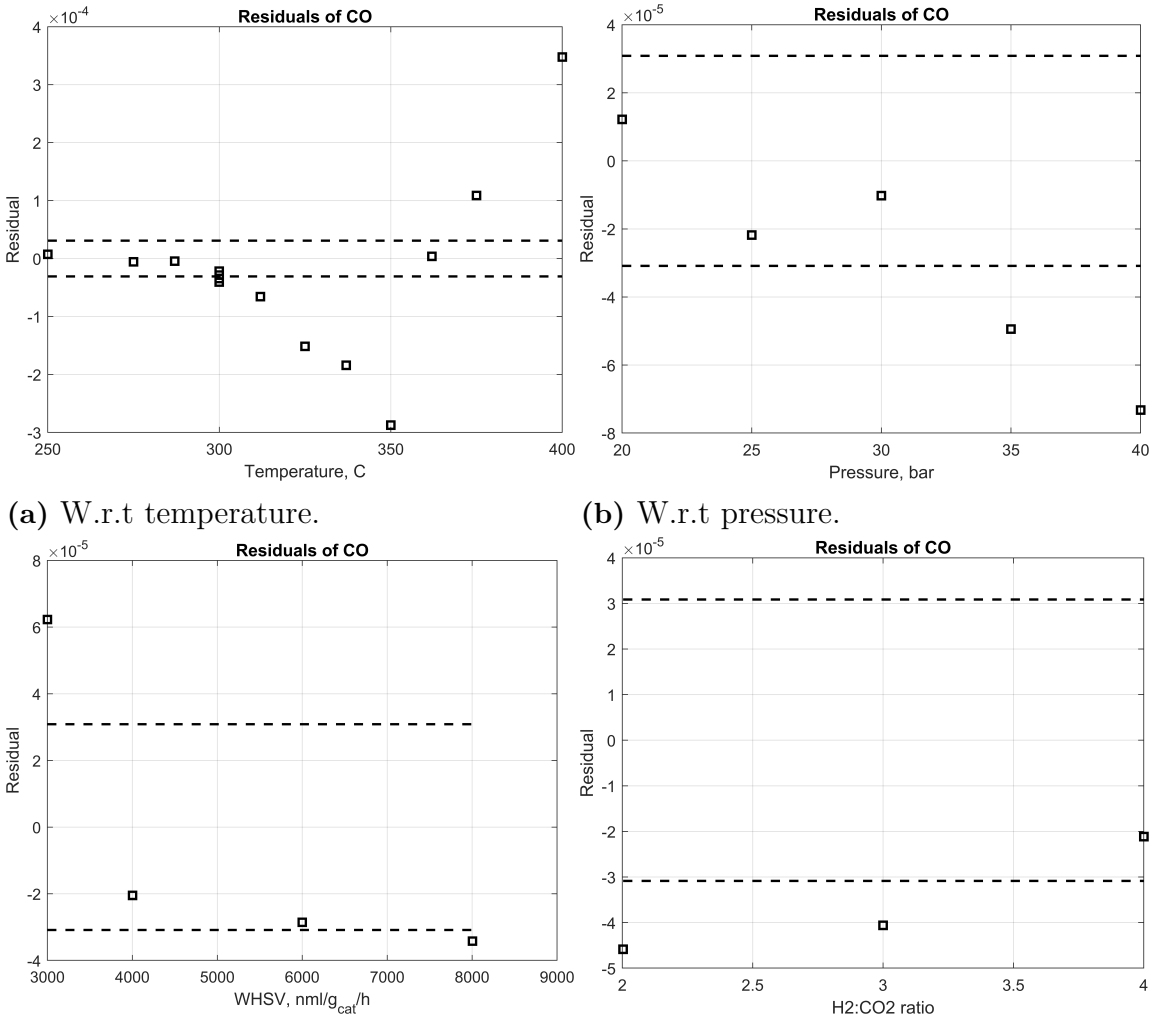


Figure B.14: Residuals of methane defined in equation 3.23 over the chronological order of the experiments were conducted.

B.2.5 CO residual plots



(a) W.r.t temperature.

(b) W.r.t pressure.

(c) W.r.t WHSV

(d) W.r.t H_2:CO_2 ratio

Figure B.15: Residual plots defined in equation 3.23 of CO over different reactor conditions

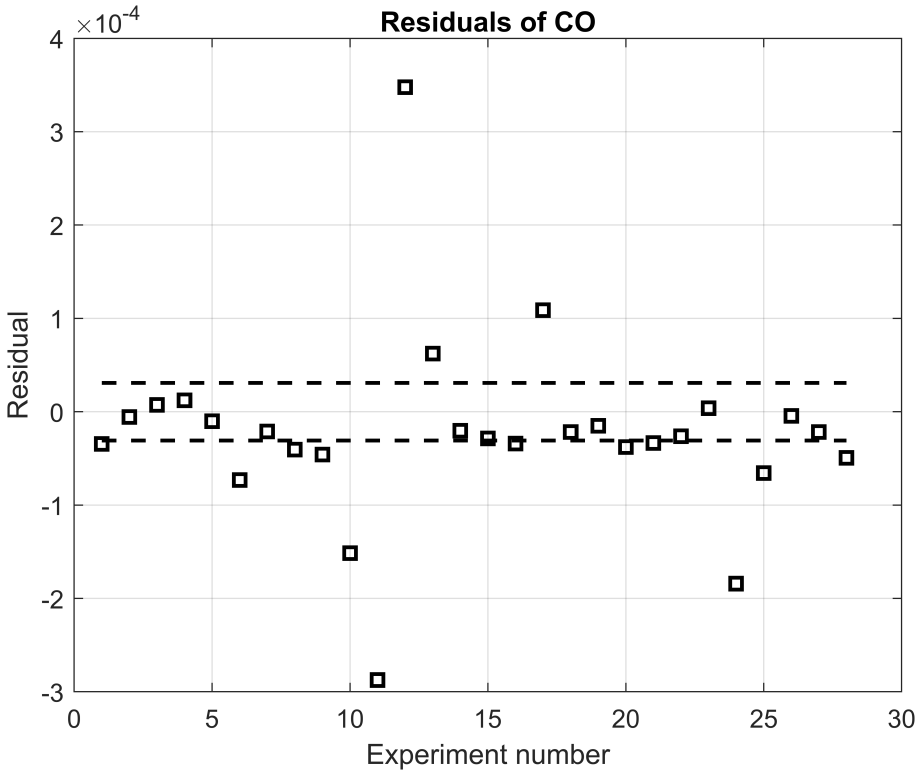
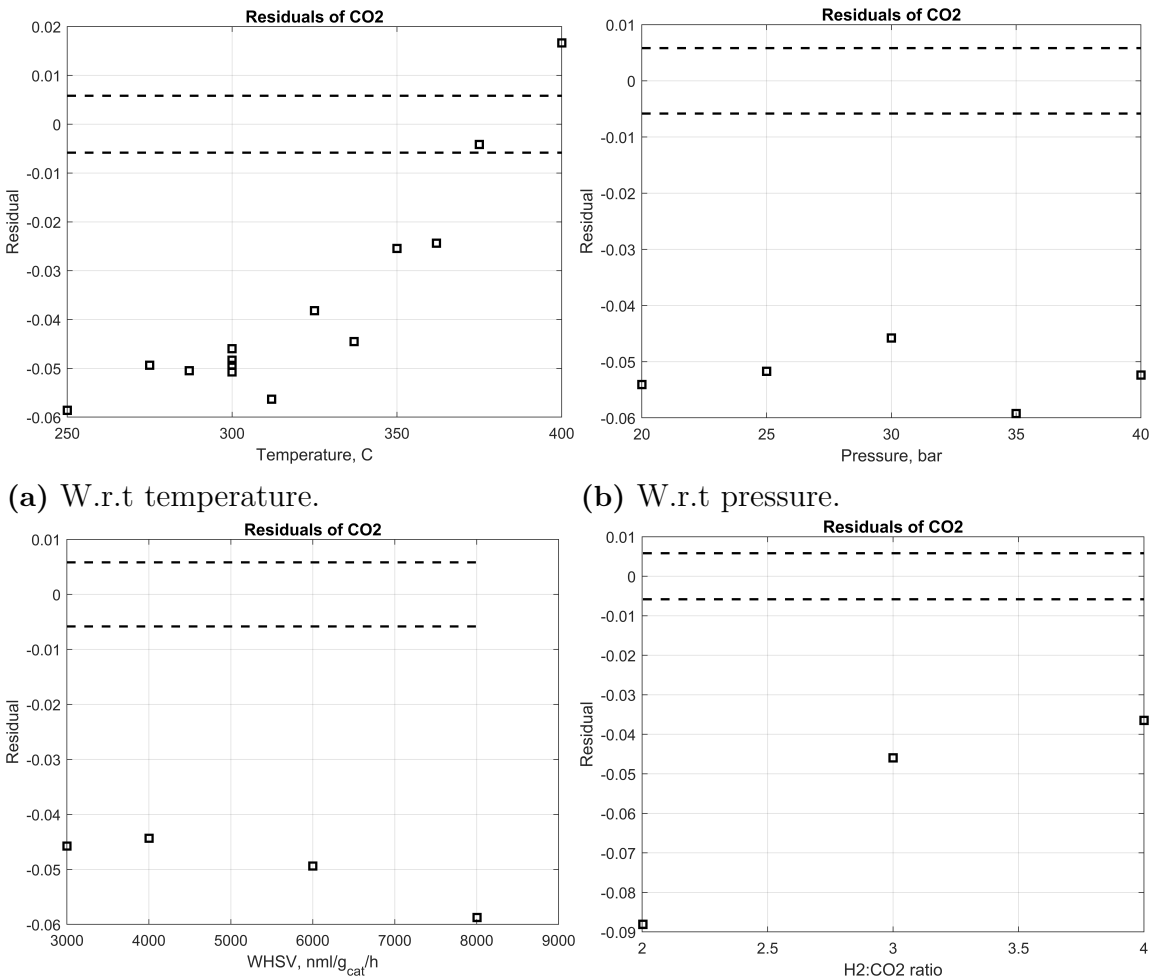


Figure B.16: Residuals of CO defined in equation 3.23 over the chronological order of the experiments were conducted.

B.2.6 CO_2 residual plots



(a) W.r.t temperature.

(b) W.r.t pressure.

(c) W.r.t WHSV

(d) W.r.t H_2:CO_2 ratio

Figure B.17: Residual plots as defined in equation 3.23 of CO_2 over different reactor conditions

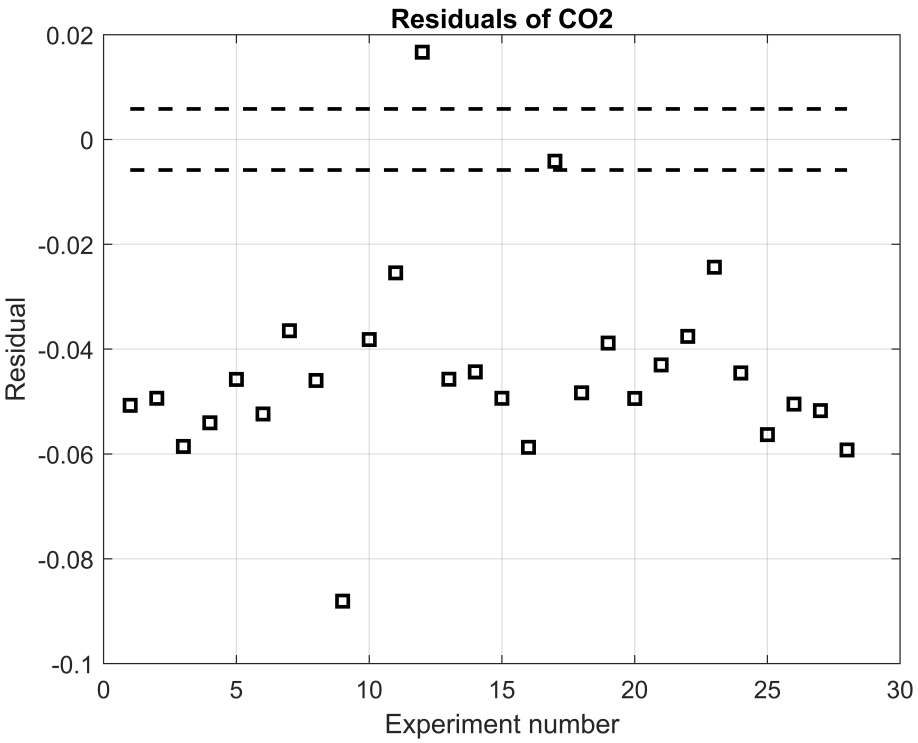


Figure B.18: Residuals of CO_2 defined in equation 3.23 over the chronological order of the experiments was conducted.

C

Appendix - Mass transfer model

During the creation of this thesis there were issues with the gas chromatograph that had to be solved before experiments could be conducted. This problem was prolonged much longer than anticipated and therefore an alternative work was initiated and worked on for approximately 1 week before the problem was fixed and the alternative work was put to the side. The alternative work was to develop a model for heterogeneous catalysis where inner and outer mass transfer was taken into account in order to evaluate the effect that mass transfer has on the CO_2 hydrogenation to methanol.

C.1 Model description

The model is a bit more complicated than the model used for developing the kinetic model. It consists of two parts, one differential plug flow reactor model and one model for the catalyst particles.

C.1.1 Reactor model

The reactor is modelled as a one dimensional plug flow reactor with the the following assumptions:

- Isothermal conditions
- Isobaric condtions
- Steady state
- Negligble axial dispersion

A mass balance over a disc control volume with the length Δx and interfacial area A gives us the model.

$$0 = F\Big|_x - F\Big|_{x+\Delta x} + N \cdot S \cdot V \tag{C.1}$$

Where F is the molar flow, N is the molar flux in/out to the catalyst, S is the specific surface area of the catalyst and V is the volume of the control volume.

$$V = \varepsilon \cdot A \cdot \Delta x \tag{C.2}$$

Where ε is the packed bed void fraction and A is the cross sectional area of the reactor. Then equation C.1 becomes

$$0 = \frac{F\Big|_x - F\Big|_{x+\Delta x}}{\Delta x} + N \cdot S \cdot \varepsilon \cdot A \tag{C.3}$$

Let $\Delta x \longrightarrow 0$

$$0 = -\frac{dF}{dx} + N \cdot S \cdot \varepsilon \cdot A \tag{C.4}$$

Rearranging

$$\frac{dF}{dx} = N \cdot S \cdot \varepsilon \cdot A \tag{C.5}$$

Equation C.5 is the final model used that will be solved. The flux of the species is

$$N = \Gamma_n (C_{bulk} - C_{surface}) \tag{C.6}$$

Where Γ_n is a lumped transport coefficient for the outermost layer of the catalyst. This is dependent on the model for the catalyst particle. So to calculate that the catalyst model is required. $C_{surface}$ is calculated from the catalyst particle model and is the concentration on the outermost layer of the catalyst.

C.1.2 Catalyst particle model

The catalyst particle model is done by discretising the catalyst particle into n amount of shells where shell n is the outermost shell and shell *1* is the centre of the catalyst particle. Then the model for one shell i is then

$$\frac{dC_i}{dt} = -\frac{\Gamma_{i-1}}{V_i}(C_i - C_{i-1}) + \frac{\Gamma_i}{V_i}(C_{i+1} - C_i) + \rho_c \sum_j \nu_j r_{i,j} \tag{C.7}$$

Where C_i is the concentration in shell i, V_i is the volume of shell i, ρ_c is the density of the catalyst, ν_j is the stoichiometric coefficient of the specie in reaction j, $r_{i,j}$ is the reaction rate of reaction j in shell layer i and Γ_i is a lumped transport coefficient that can vary. If $i = n$ then

$$\Gamma_n = \frac{A_n}{\frac{1}{k_c} + \frac{0.5\delta_n}{D_{eff}}} \tag{C.8}$$

Where A_n is outer the surface area of shell n, k_c is the convective mass transfer coefficient, which is calculated in the same manner as in appendix A, D_{eff} is the effective diffusivity and is assumed to be a tenth of the molecular diffusivity which is calculated in the same way as in appendix A and δ_n is the thickness of shell n. For $n - 1 > i \geq 1$ we have instead

$$\Gamma_i = \frac{D_{eff} A_i}{0.5\delta_i + 0.5\delta_{i+1}}. \tag{C.9}$$

Lastly, $\Gamma_0 = 0$ since it corresponds to the centre of the catalyst particle, where no net flux of species should occur. With this information a series of ODEs corresponding to one species in each layer

C.1.3 Model Implementation

The model was implemented using the kinetic model that Ghosh *et al.* developed for CO_2 hydrogenation to methanol. The main equation solved was equation 3.6 which

in itself contained a series of ODE to solve for each catalytic layer and species. For the catalytic layer the steady state solutions were found using ODE15s and letting the calculation go until time changes were negligible and then use that information to calculated Γ_n for equation 3.6. For the simulations the following data and assumptions were used.

- Inlet flow was $5.57{\cdot}10^{-5}$ mol/s H_2 and $1.86{\cdot}10^{-5}$ mol/s CO_2
- Temperature was 300 °C
- Total pressure was 40 bars
- Reactor diameter was 1.27 cm.
- Reactor length was 0.1 m
- Catalyst particle diameter was 10 mm
- Catalyst density was 2000 kg/m^3
- Packed bed void fraction was 0.35

C.2 Results

It of most interest to see how the concentration of different species varies inside of the catalyst if there is a great. Therefore, the concentration of various species over distance from catalyst particle centre is shown in figure C.1.

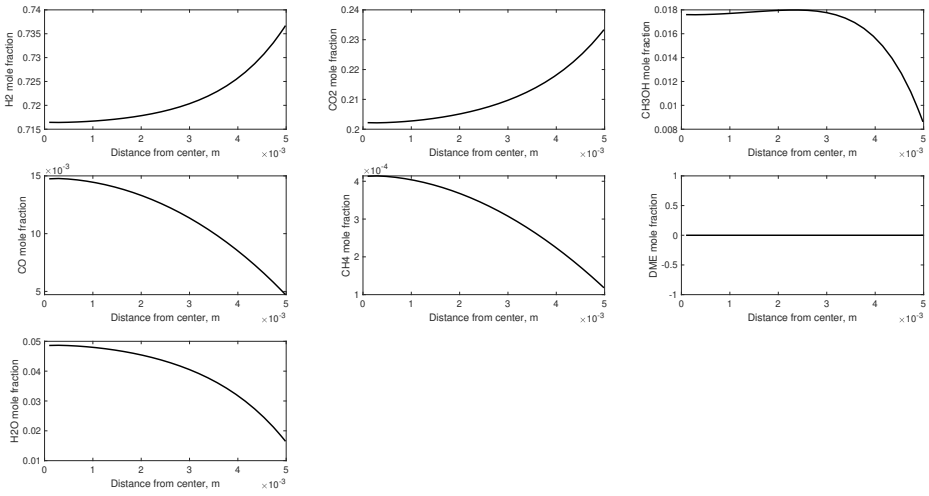
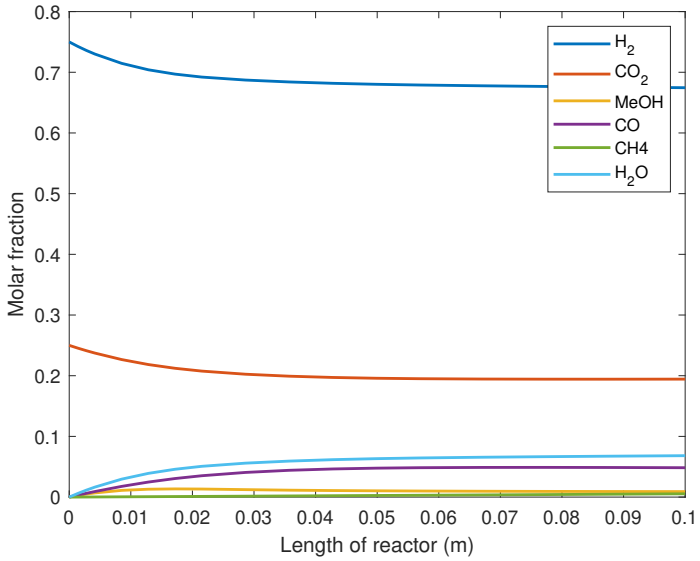


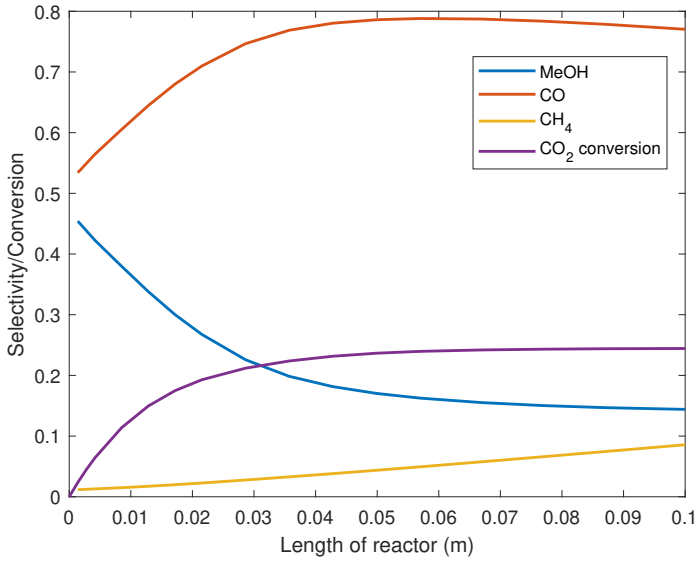
Figure C.1: Concentration over length from catalyst centre of various species. From top left: H_2, CO_2, MeOH, CO, CH_4, DME and H_2O.

Figure C.1 shows that the model seems to work as intended. The largest concentration of products and the smallest concentration of reactants are in the centre of the catalyst. As the catalyst particle has been set to a very large diameter there should be very significant mass transfer limitations in the system. For the methanol the concentration is relatively constant at a distance from the centre below 3 mm. This means that a lot of the catalyst is in equilibrium and that only a part of the catalyst is used for synthesising methanol. Therefore, there are reasons to believe

there can be mass transfer limitation for methanol synthesis. The results for the reactor simulation are shown in figure C.2



(a) Molar fraction in the simulated reactor.



(b) Selectivities and CO_2 conversion of the simulated reactor

Figure C.2: Reactor simulation results.

The most striking thing about figure C.2b is that the CO_2 conversion will not be much higher than 24% since both methanol synthesis and RWGS have reached equilibrium.

DEPARTMENT OF SOME SUBJECT OR TECHNOLOGY
CHALMERS UNIVERSITY OF TECHNOLOGY
Gothenburg, Sweden
www.chalmers.se



CHALMERS
UNIVERSITY OF TECHNOLOGY